J. Fluid Mech. (2021), *vol*. 918, A46, doi:10.1017/jfm.2021.355

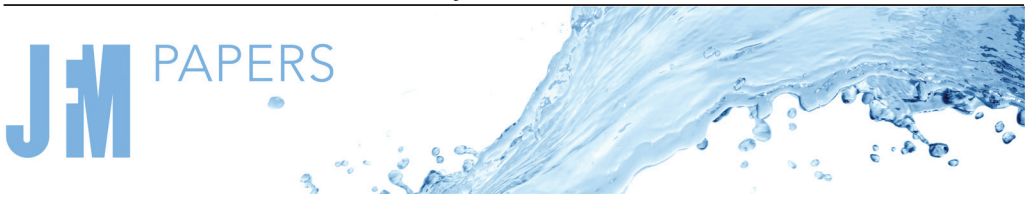

Sound scattering by a vortex: case of exponentially decaying velocity

Dmitry A. Gadzhiev[1,2,†] **and Alexander M. Gaifullin**[1,2]

[1]Phystech School of Aerospace Technology, Moscow Institute of Physics and Technology, 9 Institutskiy per., Dolgoprudny, Moscow Region 141701, Russian Federation

[2]Central Aerohydrodynamic Institute, 1 Zhukovsky Street, Zhukovsky, Moscow Region 140180, Russian Federation

(Received 31 August 2020; revised 28 March 2021; accepted 16 April 2021)

The well-known two-dimensional problem of a plane acoustic wave scattering by a point vortex is ill-posed because the vortex velocity field decays as r^{-1} at infinity. We show that for problem to be well-posed, the velocity field must decay more rapidly than as $r^{-3/2}$. We propose a reformulation where the point vortex is screened by a vortical mantle with the opposite total circulation such that the velocity field is proportional to $r^{-1}\exp(-r^2/L^2)$. The vortex effective radius L is assumed long compared with the acoustic wavelength λ. In the Born approximation, the scattered field is the solution to the inhomogeneous Helmholtz equation with the Sommerfeld radiation condition that can be represented as convolution of the source term with Green's function. The asymptotic evaluation as $\lambda/L \to 0$ shows the analogy to plane-wave diffraction by a slit of width L. In the Fraunhofer region $r \gg L^2/\lambda$, the solution is an outgoing cylindrical wave that peaks at small scattering angles $\theta = O(\lambda/L)$ and matches the expression with a singularity on $\theta = 0$ known from the case of the point vortex (Pitaevskii, *Sov. Phys. JETP*, vol. 8, 1959, pp. 888–890) as $\theta \gg \lambda/L$. In a part of the region of geometrical acoustics $r \ll L^2/\lambda$ including the region $r \ll L$ where the vortex velocity field is proportional to r^{-1}, the solution matches the second known expression (Sakov, *Acoust. Phys.*, vol. 39, 1993, pp. 280–282) that does not decay at infinity. The results are confirmed by numerical integration.

Key words: aeroacoustics, wave scattering

1. Introduction

The problem of wave scattering by vortices has been extensively studied since the 1950s, arising from various branches of physics. Lighthill (1953) studied sound generation

† Email address for correspondence: gadzhiev@phystech.edu

and scattering by a turbulent flow in the framework of the linearised Euler equations. Pitaevskii (1959) used the equivalent approach for sound scattering by a vortex filament to calculate the phonon part of the mutual friction force between the normal fluid and the superfluid components of helium II. Aharonov & Bohm (1959) discovered the significance of electromagnetic potentials in quantum mechanics by solving the Schrödinger equation for an electron beam scattering by a magnetic field whose vector potential was organised like the vortex-filament velocity field. Howe (1975) developed a theory of aerodynamic noise generated by a jet and theory of the flute. Golemshtok & Fabricant (1980) examined sound scattering by the Rankine vortex including the resonant case for studying its acoustic instability. Kopiev & Leontiev (1987) included it as an auxiliary case for studying the acoustic instability of, and sound radiation by, a vortex ring. Coste, Lund & Umeki (1999) considered the scattering of surface gravity waves by vertical vorticity in shallow water governed by linearised shallow water equations. Smith (2002) studied acoustic wave scattering by a superfluid vortex using the linearised Gross–Pitaevskii equation, whereas Wei *et al.* (2017) investigated electromagnetic waves in a liquid using Maxwell's equations. In the framework of the Born approximation, which takes place for weak vortices, the inhomogeneous wave equation governing the scattered field is equivalent for equivalent incident waves and vortices of different nature if rewritten in corresponding quantities. Thus, Berry *et al.* (1980) and Coste *et al.* (1999) showed the analogy of the Aharonov–Bohm effect for surface water waves, whereas Reinschke, Möhring & Obermeier (1997) showed the analogy between quantum-mechanical and acoustic scattering. Lindsay (1948) and Salant (1969) developed the approach within the framework of the geometrical (ray) acoustics, when the wavelength is assumed equal to zero and trajectories of individual sound rays in the phase space are of interest. This approach implied solving the Hamiltonian equations for the wave frequency dependent on the position and the wave vector. Using this, Nazarenko (1994); Nazarenko, Zabusky & Scheidegger (1995) discovered sound absorption by thin vortex filaments, meaning that acoustic rays can collapse on to the vortex core without reflection.

In this paper we deal with acoustic waves in an inviscid ideal gas. For brevity, we use the notation $\boldsymbol{U}$ instead of density ρ, pressure p, and velocity $\boldsymbol{v}$ in equations related to any of them and denote the vortex field by $\boldsymbol{U}_{vort}$, the incident acoustic field by $\boldsymbol{U}_{inc}$ and the scattered acoustic field by $\boldsymbol{U}_{scat}$. The scattered field represents the addition to the superposition of the vortex and the incident field owing to their interaction, defined as follows:

$$\boldsymbol{U} = \boldsymbol{U}_{vort} + \boldsymbol{U}_{inc} + \boldsymbol{U}_{scat}. \tag{1.1}$$

There are many examples of scattering problems in aeroacoustics that have been successfully solved in the Born approximation

$$|\boldsymbol{U}_{scat}| \ll |\boldsymbol{U}_{inc}|. \tag{1.2}$$

For the case when the incident field is the uniform monochromatic plane acoustic wave

$$\rho_{inc} \propto p_{inc} \propto \exp(\mathrm{i}(\boldsymbol{k}\cdot\boldsymbol{r} - \omega t)) + \text{c.c.}, \quad \boldsymbol{v}_{inc} \propto \hat{\boldsymbol{k}}\rho_{inc} \tag{1.3a,b}$$

of a small amplitude, Kambe & Oo (1981) and Howe (1983) solved the problem for the vortex ring, Tanaka & Ishii (1982) for the vortex pair, Gromov, Ezerskii & Fabrikant (1982) for the Kármán vortex street, Fabrikant (1983) for a general two-dimensional zero-circulation flow, Klimov & Prozorovskii (1987) for Hill's vortex, Colonius, Lele & Moin (1994) for the Taylor vortex (numerically), Smith & Ford (2001) for a

general three-dimensional flow and Naugolnykh (2013) for the Lamb–Chaplygin dipole. In these cases, the Sommerfeld radiation condition (see Schot 1992) ensures that the solution to the wave equation is unique (Sveshnikov, Bogolyubov & Kravtsov 2004, § VIII.6) and in the far field represents an outgoing wave. In the case of a two-dimensional steady flow, this is a cylindrical wave

$$\rho_{scat} \propto p_{scat} \propto \frac{\exp(\mathrm{i}(kr-\omega t))}{\sqrt{kr}} f(\theta), \quad \boldsymbol{v}_{scat} \propto \hat{\boldsymbol{r}}\rho_{scat}. \tag{1.4a,b}$$

Here t is time, $\boldsymbol{r}$ is the position vector, r and θ are polar coordinates, ω is the angular frequency, $\boldsymbol{k}$ is the wave vector of the incident wave, $\hat{\boldsymbol{r}} = \boldsymbol{r}/r$, $\hat{\boldsymbol{k}} = \boldsymbol{k}/k$ and c.c. is the complex conjugate part, dropped hereafter. The solution (1.4) agrees with the conservation of the total scattered energy flux (Landau & Lifshitz 1987, § 78)

$$W_{scat}(r) \propto \int_{-\pi}^{\pi} |\boldsymbol{v}_{scat}|^2 r \,\mathrm{d}\theta \propto \int_{-\pi}^{\pi} f^2(\theta)\,\mathrm{d}\theta. \tag{1.5}$$

Most of the cited papers, however, address one specific two-dimensional case such that the incident field is (1.3), whereas the flow is an axisymmetric vortex,

$$\rho_{vort} = \rho_{vort}(r), \quad p_{vort} = p_{vort}(r), \quad \boldsymbol{v}_{vort} = \frac{\Gamma(r)}{2\pi r}\hat{\boldsymbol{\theta}}, \tag{1.6a–c}$$

for which the total circulation is non-zero and vorticity is localised within a region short compared with the acoustic wavelength such that

$$\Gamma(r) \to \Gamma_* > 0 \quad \text{as } r/r_* \to \infty, \quad kr_* \ll 1. \tag{1.7}$$

Here $\hat{\boldsymbol{\theta}}$ is the unit vector orthogonal to $\hat{\boldsymbol{r}}$; the position vector $\boldsymbol{r}$ is hereafter measured from the vortex centre, whereas the scattering angle $\theta \in [-\pi; \pi]$ from the direction of incidence $\hat{\boldsymbol{k}}$. The distributions (1.6) are assumed to obey the compressible Euler equations. We do not distinguish between vortices with different $\Gamma(r)$ as $r/r_* = O(1)$, such as the point vortex, the Rankine vortex and the Lamb–Oseen vortex, as this does not affect the solution in the Born approximation (Howe 1999). For the case (1.3), (1.6), (1.7) referred to as plane wave, point vortex (PWPV), there are two radically different results as $kr \to \infty$. Pitaevskii (1959), Fetter (1964), Ferziger (1974), O'Shea (1975), Candel (1979), Fabrikant (1983), Kopiev & Leontiev (1987) and Colonius *et al.* (1994) obtained a cylindrical wave (1.4) with scattering amplitude

$$f(\theta) \propto \cos\theta \cot\frac{\theta}{2}, \tag{1.8}$$

having a singularity in the direction $\theta = 0$. Sakov (1993), Ford & Smith (1999), Howe (1999) and Kopiev & Belyaev (2010) obtained a field that was regular but non-decaying at infinity, so that

$$\max_{\theta} |\boldsymbol{U}_{scat}| \to \text{const} \quad \text{as } kr \to \infty. \tag{1.9}$$

We will refer to the expressions corresponding to two previous equations as follows: the former as expression (i), and the latter as expression (ii); exact equations will be written out in § 5. Much earlier Aharonov & Bohm (1959) and Berry *et al.* (1980) obtained an expression very similar to (ii), yet for a special case beyond the Born approximation. Coste *et al.* (1999) provided an analogous solution for the case $kr_* \gg 1$.

By direct substitution into the governing inhomogeneous wave equation, one can ensure that only expression (ii) is actually its solution, whereas expression (i) is not, because in the leading-order approximation it obeys the homogeneous wave equation and so is definitely incorrect. In addition, numerical (Candel 1979; Colonius *et al.* 1994; Berthet, Fauve & Labbé 2003; Karabasov, Kopiev & Goloviznin 2009; Doronina & Zhdanova 2013; Iwatsu & Tsuru 2013; Clair & Gabard 2015) and experimental (Berry *et al.* 1980; Horne 1983; Labbe & Pinton 1998; Vivanco *et al.* 1999; Manneville *et al.* 2001) results for acoustic and surface water waves strongly disproved expression (i) and were qualitatively comparable to expression (ii) in cases corresponding to the Born approximation. Expression (ii) also raises some doubts because it possesses an unlimited total scattered energy flux (1.5). A regular solution having the form (1.4) is still unknown.

The problem with case PWPV is related to the fact recognised by Colonius *et al.* (1994), Berthet & Lund (1995), Reinschke *et al.* (1997) and Belyaev & Kopiev (2008), namely, that the respective scattering problem with the Sommerfeld radiation condition is ill-posed. This is a consequence of the infinite range of the wave–vortex interaction. More precisely, the source term in the wave equation decays proportionally to $|\boldsymbol{v}_{vort}| \propto r^{-1}$ as $r/r_* \to \infty$, which is insufficient for this problem to be well posed. To deal with the well-posed problem, one needs a proper condition that will act as a regularisation. Enforcing the radiation condition despite the aforementioned led to expression (i). Applying regularisations led to expression (ii). However, Belyaev & Kopiev (2008) noticed that the applied regularisations were still incorrect. Indeed, all of them used assumptions that were not actually fulfilled by expression (ii). Sakov (1993) dealt with divergent integrals dependent on the method of integration. Ford & Smith (1999) and Howe (1999) imposed the causality condition that the incident wavenumber had an infinitely small positive imaginary part, $k \to k + \mathrm{i}0$, which was in fact the consequence of the limiting absorption principle (Sveshnikov *et al.* 2004, § VIII.6) equivalent to the radiation condition. Nevertheless, they still incorrectly assumed decaying at infinity (see § 5.4) in contrast to (1.9). Aharonov & Bohm (1959), Berry *et al.* (1980) and Coste *et al.* (1999) assumed an outgoing wave plus additional terms owing to the incident wave refraction by the flow, which was violated by expression (ii) at small scattering angles. Thus, all known formulations seem to fail, and perhaps the problem of the plane acoustic wave scattering by a vortex with non-zero total circulation is fundamentally ill-posed, even beyond the Born approximation (Aharonov & Bohm 1959; Berry *et al.* 1980; Coste *et al.* 1999).

The ill-posed nature of the problem for case PWPV means that a uniform plane wave (1.3) scattering by an axisymmetric vortex (1.6) with non-zero total circulation (1.7) is ambiguous. The observed scattered field in a physical or numerical experiment will depend on the actual incident field and flow and may be different for different implementations (see discussion by Kopiev & Belyaev 2010). Some researchers who recognised that this problem is ill-posed proposed changing the physical statement of the problem, precisely, to confine the region of interaction, in order to make use of the radiation condition. Berthet & Lund (1995) proposed two options: one, cut off the vortex velocity field by the factor $\exp(-r/L)$, the other, cut off the incident wave by $\exp(-y^2/L^2)$, where $y = r\sin\theta$ is the Cartesian coordinate along the incident wavefront. For both cases they obtained regular solutions having the form (1.4); however, in the limit $L \to \infty$ corresponding to case PWPV both were similar to the incorrect expression (i) rather than to (ii). Reinschke *et al.* (1997) assumed the fluid to rest in the region $r > L$. Kopiev & Belyaev (2010) proposed replacing the plane wave (1.3) with a cylindrical wave emitted by a point source at a finite distance

from the vortex centre. They obtained expression (ii) in a limited region beyond the Born approximation; however, it is not obvious whether their solution decomposed into a Fourier series by angle θ was a purely outgoing wave (1.4) in the far field. As noted by Belyaev & Kopiev (2008), the far-field expansion of the Bessel function can be used only when its argument is much greater than its index, which is not the case for the infinite series. An uncontroversial solution is still unknown.

The goal of this paper is the formulation and the solution in the Born approximation of a well-posed scattering problem that can be considered a natural analogue to the problem of a plane acoustic wave scattering by a point vortex, in a similar manner to that carried out by Berthet & Lund (1995). In § 2 we outline the structure of the solution with the specification of basic concepts, with particular attention to the meaning of 'incident field' and 'scattered field'. In § 3 we examine the well-posedness of the scattering problem in the Born approximation with the radiation condition for a general incident acoustic wave and a general vortex. In § 4 we propose the appropriate formulation of the problem using a new model for the vortex, present the way it can be implemented and define the validity of the framework used. In § 5 we analyse the solution to the well-posed problem and its relationship with expressions (i), (ii) and with the solution by Berthet & Lund (1995). The solution obtained constitutes the main importance of the present work. In § 6 we give the summary and discuss the sense of the work undertaken in the context of the original question.

2. Structure of the total field

Let us consider the general scattering problem when a small-amplitude monochromatic acoustic wave

$$\boldsymbol{U}_{inc} = \boldsymbol{\mathcal{U}}_{inc}(\boldsymbol{r})\,\mathrm{e}^{-\mathrm{i}\omega t} \tag{2.1}$$

propagates through a steady flow

$$\boldsymbol{U}_{vort} = \boldsymbol{U}_{vort}(\boldsymbol{r}) \tag{2.2}$$

of an inviscid ideal gas. We move to the dimensionless variables

$$\bar{\rho} = \rho/\rho_\infty, \quad \bar{p} = p/p_\infty, \quad \bar{\boldsymbol{v}} = \boldsymbol{v}/c_\infty, \quad \bar{t} = \omega t, \quad \bar{\boldsymbol{r}} = k\boldsymbol{r}, \tag{2.3a–e}$$

where ρ_∞, p_∞, $c_\infty = \sqrt{\gamma p_\infty/\rho_\infty}$ are the unperturbed gas density, pressure and sound speed, ω is the angular frequency, $k = \omega/c_\infty$ is the wavenumber of the incident wave and γ is the heat capacity ratio; the overlines are dropped hereafter. The Euler equations are

$$\frac{\partial \rho}{\partial t} + \boldsymbol{\nabla}\cdot(\rho\boldsymbol{v}) = 0, \tag{2.4a}$$

$$\frac{\partial \boldsymbol{v}}{\partial t} + \boldsymbol{v}\cdot\boldsymbol{\nabla}\boldsymbol{v} + \frac{1}{\gamma}\frac{\boldsymbol{\nabla} p}{\rho} = 0, \tag{2.4b}$$

$$\frac{\partial}{\partial t}\frac{p}{\rho^\gamma} + \boldsymbol{v}\cdot\boldsymbol{\nabla}\frac{p}{\rho^\gamma} = 0. \tag{2.4c}$$

In addition to the incident wave amplitude, to apply the Born approximation (1.2) we assume that the flow Mach numbers are also small, giving

$$a = \max|\boldsymbol{v}_{inc}| \ll 1, \tag{2.5a}$$

$$M = \max|\boldsymbol{v}_{vort}| \ll 1. \tag{2.5b}$$

The formulation (2.1)–(2.5) suggests that the solution to equations (2.4) can be decomposed into a two-parameter series by M and a. As soon as we neglect terms $O(a^2)$ which are related to the self-convection of waves, and to the wave-induced remote recoil forces (Bühler & McIntyre 2003), the complex conjugate part can be dropped, as in (2.1). Then the solution depends on the parameter a and time t only as on the combination $a\,\mathrm{e}^{-\mathrm{i}t}$, giving

$$\boldsymbol{U} = \sum_{i=0}^{\infty}\sum_{j=0}^{1} M^i (a\,\mathrm{e}^{-\mathrm{i}t})^j \boldsymbol{U}_{ij}(\boldsymbol{r}) + \text{h.o.t.}, \tag{2.6}$$

where h.o.t. includes non-power terms that may appear at higher orders.

The time-independent part of (2.6) represents the flow field

$$\boldsymbol{U}_{vort} = \sum_{i=0}^{\infty} M^i \boldsymbol{U}_{i0}(\boldsymbol{r}). \tag{2.7}$$

The solution at $O(1)$ is the unperturbed fluid

$$\rho_{00} = p_{00} = 1, \quad \boldsymbol{v}_{00} = 0. \tag{2.8a,b}$$

If the pressure and density fields are perturbed only by the flow, they consist of even powers of the Mach number, such that

$$\rho_{vort} = 1 + M^2 \rho_{20}(\boldsymbol{r}) + O(M^4), \quad p_{vort} = 1 + M^2 p_{20}(\boldsymbol{r}) + O(M^4), \tag{2.9a,b}$$

whereas for the velocity field the powers are odd as follows

$$\boldsymbol{v}_{vort} = M \boldsymbol{v}_{10}(\boldsymbol{r}) + O(M^3). \tag{2.10}$$

In the leading-order approximation the flow is incompressible, as

$$\nabla \cdot \boldsymbol{v}_{10} = 0. \tag{2.11}$$

The time-dependent part of (2.6) represents the acoustic field

$$\boldsymbol{U}_{inc} + \boldsymbol{U}_{scat} = a\,\mathrm{e}^{-\mathrm{i}t} \sum_{i=0}^{\infty} M^i \boldsymbol{U}_{i1}(\boldsymbol{r}) + \text{h.o.t.} \tag{2.12}$$

The incident field is the flow-independent part of (2.12)

$$\boldsymbol{U}_{inc} = a \boldsymbol{U}_{01}(\boldsymbol{r})\,\mathrm{e}^{-\mathrm{i}t}, \tag{2.13}$$

whereas the scattered field constitutes the remainder

$$\boldsymbol{U}_{scat} = a\,\mathrm{e}^{-\mathrm{i}t} \sum_{i=1}^{\infty} M^i \boldsymbol{U}_{i1}(\boldsymbol{r}) + \text{h.o.t.} \tag{2.14}$$

Thus, the sum of 'pure' components (2.7) + (2.13) represents the superposition of the flow field and the incident acoustic field, and is given. The sum of 'mixed' components (2.14) represents the product of their interaction, the scattered field, and needs to be

determined. As long as the representation by a power series is uniformly valid, either of the components satisfies the equations derived by the substitution of (2.6) into (2.4)

$$(\nabla^2 + j^2)\rho_{ij} = q^{\rho}_{ij}, \quad (\nabla^2 + j^2)p_{ij} = q^{p}_{ij}, \quad \boldsymbol{\nabla}(\boldsymbol{\nabla}\cdot\boldsymbol{v}_{ij}) + j^2\boldsymbol{v}_{ij} = \boldsymbol{q}^{\boldsymbol{v}}_{ij}, \tag{2.15a–c}$$

where $\boldsymbol{q}^{\boldsymbol{U}}_{ij}(\boldsymbol{r})$ are known functions resulting from the interaction between the lower-order components, meaning those with the first index less than or equal to i and the second index less than or equal to j. For the incident field (2.13), equations (2.15) are homogeneous. The boundary conditions are specified for each component individually.

This means that we regard the flow and the incident wave as two interacting small perturbations (vortical and acoustic mode, respectively), whereas the unperturbed fluid (2.8) as the background state. The validity of this framework is ensured by the assumptions (2.5). The similar approach was developed by Ford & Smith (1999), Bühler & McIntyre (2003) and McIntyre (2019), who, in addition, assumed $a \ll M$. It is more consistent than the commonly used framework (including in scattering problems beyond aeroacoustics) when the acoustic wave is assumed a small perturbation against the background flow, i.e.

$$|\boldsymbol{U}_{inc}| \ll |\boldsymbol{U}_{vort}|, \tag{2.16}$$

and equations (2.4) are linearised with respect to $\boldsymbol{U}_{vort}$. Indeed, the assumption (2.16) breaks down in cases such as PWPV when $\boldsymbol{v}_{vort} \to 0$ as $r \to \infty$, whereas $|\boldsymbol{v}_{inc}| = \text{const}$. This point is relevant for waves of different nature, e.g. near-inertial waves in geostrophic flows (Balmforth, Smith & Young 1998; Smith 1999; Thomas, Smith & Bühler 2017), waves in shallow-water rotating flows (Ford 1994; McIntyre 2009) and in stratified flows (Plougonven & Zeitlin 2002). However, the relative magnitude of the flow field $O(M)$ and the incident acoustic field $O(a)$ does not actually matter, because neither $\boldsymbol{U}_{10}$ nor $\boldsymbol{U}_{01}$ depend on another via the source term in (2.15). Owing to this, on the one hand the additional assumption $a \ll M$ made by Ford & Smith (1999), Bühler & McIntyre (2003) and McIntyre (2019) was redundant, and on the other hand the breakdown of the assumption (2.16) did not lead to the breakdown of the solution.

The representation by a power series and, hence, equations (2.15) is uniformly valid as long as

$$M|\boldsymbol{U}_{i+1,1}| \ll |\boldsymbol{U}_{i1}|. \tag{2.17}$$

The Born approximation (1.2) assumes (2.17) for the leading-order scattered field, giving

$$M|\boldsymbol{U}_{11}| \ll |\boldsymbol{U}_{01}|. \tag{2.18}$$

The presence of multiple spatial scales in (2.1) and (2.2) may cause $|\boldsymbol{U}_{i+1,1}| \gg 1$, which may lead to the breakdown of (2.17) and non-power terms appearing at higher orders in (2.14). For instance, Ford & Smith (1999) discovered higher-order terms $O(M^i a \ln M)$ in case PWPV, appearing as a consequence of the logarithmic behaviour of Green's function for equations (2.15) in the near limit. Meanwhile, the condition $a|\boldsymbol{U}_{i1}| \ll |\boldsymbol{U}_{i0}|$, similar to (2.17), is not required, because $\boldsymbol{U}_{i1}$ and $\boldsymbol{U}_{i0}$ depend on time differently.

2.1. *Definition of the incident and scattered wave*

The separation of the total acoustic field (2.12) into incident and scattered components is actually a non-trivial issue that may seem ambiguous, as highlighted in the review by Sakov (1993). In a physical experiment, the measurable quantities are the amplitude A and the phase φ of the total acoustic field (see Manneville *et al.* 2001; Berthet *et al.* 2003),

rather than the amplitude and the phase of the incident or scattered field separately. For simplicity, let us associate them to the density field by

$$\rho_{inc} + \rho_{scat} \equiv aA\,\mathrm{e}^{\mathrm{i}(\varphi - t)}, \tag{2.19}$$

and decompose into a series by M, giving

$$A = \sum_{i=0}^{\infty} M^i A_i(\boldsymbol{r}) + \text{h.o.t.}, \quad \varphi = \sum_{i=0}^{\infty} M^i \varphi_i(\boldsymbol{r}) + \text{h.o.t.} \tag{2.20a,b}$$

Comparing (2.19) and (2.20) with (2.12), we obtain the leading-order approximation

$$A_0 = |\rho_{01}|, \quad \varphi_0 = \arg \rho_{01} \tag{2.21a,b}$$

as well as the linear correction owing to the interaction with the flow

$$A_1/A_0 = \mathrm{Re}\,(\rho_{11}/\rho_{01})\,, \quad \varphi_1 = \mathrm{Im}\,(\rho_{11}/\rho_{01})\,. \tag{2.22a,b}$$

In this paper, we define the incident field by (2.13) as the given acoustic field in the absence of the mean flow $M = 0$, such that

$$|\rho_{inc}| = aA_0, \quad \arg \rho_{inc} = \varphi_0 - t, \tag{2.23a,b}$$

and the scattered field by (2.14), in the same way as Ford & Smith (1999) and Howe (1999).

Meanwhile, as O'Shea (1975) showed for the case of an axisymmetric vortex (1.6)–(1.7), the field (2.14) is the sum of two components

$$\boldsymbol{U}_{scat} = \boldsymbol{U}_{rad} + \boldsymbol{U}_{dis}, \tag{2.24}$$

the radiation of sound

$$\boldsymbol{U}_{rad} = a\,\mathrm{e}^{-\mathrm{i}t} \sum_{i=1}^{\infty} M^i \boldsymbol{U}^r_{i1}(\boldsymbol{r}) + \text{h.o.t.}, \tag{2.25}$$

and the result of the incident-wave refraction by the flow that represents the wavefront distortion

$$\boldsymbol{U}_{dis} = a\,\mathrm{e}^{-\mathrm{i}t} \sum_{i=1}^{\infty} M^i \boldsymbol{U}^d_{i1}(\boldsymbol{r}) + \text{h.o.t.} \tag{2.26}$$

We represent the linearised amplitude change and the phase shift analogously to (2.24) as $A_1 = A_1^r + A_1^d$, $\varphi_1 = \varphi_1^r + \varphi_1^d$, where all the components are defined analogously to (2.22). The distortion component $\boldsymbol{U}_{dis}$ does not interfere with the incident field, thus

$$A_1^d = 0. \tag{2.27}$$

Owing to this, Aharonov & Bohm (1959), Berry *et al.* (1980), Sakov (1993), Coste *et al.* (1999) and Kopiev & Belyaev (2010) included it in the incident field so that

$$\boldsymbol{U}'_{inc} = a\boldsymbol{U}_{01}(\boldsymbol{r})\,\mathrm{e}^{-\mathrm{i}t} + \boldsymbol{U}_{dis}. \tag{2.28}$$

The field (2.28) satisfies the inhomogeneous equations (2.15) with the higher-order source term $O(M)$ (see Blokhintsev 1946; Howe 1975) and represents the wave (2.13) distorted,

but with the same amplitude

$$|\rho'_{inc}| = aA_0, \quad \arg \rho'_{inc} = \varphi_0 - t + O(M). \tag{2.29a,b}$$

The scattered field was accordingly identified with the radiation component as

$$\boldsymbol{U}'_{scat} = \boldsymbol{U}_{rad}. \tag{2.30}$$

To summarise, existing works used two different meanings for each of the terms incident wave and scattered wave, one terminology being given by (2.13) and (2.24) and another by (2.28) and (2.30). The relative difference between the two meanings is of $O(M)$ for the incident wave and of $O(1)$ for the scattered wave.

To remove the ambiguity, we require the conservation of the total scattered energy flux (1.5) in the region where the wave–flow interaction is negligible. In § 5.3.5 we show for the relevant case that it is fulfilled only when the scattered wave is defined by (2.24). This makes the terminology (2.13), (2.24) used in this paper physically more reasonable than (2.28), (2.30).

3. Well-posedness of the scattering problem

In the Born approximation (1.2) for the case (2.1), (2.2), the leading-order approximation for the scattered field $\boldsymbol{U}_{11}(\boldsymbol{r})$ is determined by solving the inhomogeneous Helmholtz equation (2.15*a*)

$$\nabla^2 \rho_{11} + \rho_{11} = q_{11}, \tag{3.1}$$

with the source term (the index 'ρ' is dropped hereafter) simplified by taking (2.11) into account, giving

$$q_{11} = -2\frac{\partial^2 (v_{10\alpha} v_{01\beta})}{\partial r_\alpha \partial r_\beta} = -2\boldsymbol{\nabla} \cdot (\boldsymbol{v}_{10} \cdot \boldsymbol{\nabla} \boldsymbol{v}_{01}), \tag{3.2}$$

where the Greek index indicates the Cartesian component and summation over all the values α and β is implied. The source (3.2) results from the incident field interaction with the flow velocity field and represents Lighthill's (Lighthill 1953) scattering quadrupoles (Thomas 2017). The pressure and velocity fields are expressed through the density field by the substitution of (2.6) into (2.4*b*,*c*)

$$p_{11} = \gamma \rho_{11}, \quad \boldsymbol{v}_{11} = -\mathrm{i}(\boldsymbol{\nabla} \rho_{11} + \boldsymbol{v}_{10} \cdot \boldsymbol{\nabla} \boldsymbol{v}_{01} + \boldsymbol{v}_{01} \cdot \boldsymbol{\nabla} \boldsymbol{v}_{10}). \tag{3.3a,b}$$

Henceforth we consider the two-dimensional case, with a clear possible generalisation to three dimensions. Let us impose the Sommerfeld radiation condition for equation (3.1) assuming that there is a far field $r \gg r_F$ where the scattered field is an outgoing cylindrical wave (1.4*a*):

$$\frac{\partial \rho_{11}}{\partial r} - \mathrm{i}\rho_{11} = o(r^{-1/2}) \quad \text{as } r/r_F \to \infty. \tag{3.4}$$

The requirement

$$\rho_{11} = O(r^{-1/2}) \quad \text{as } r/r_F \to \infty, \tag{3.5}$$

which is often appended, is excessive because it is fulfilled for any solution of the homogeneous Helmholtz equation satisfying (3.4) (see Rellich 1943; Colonius *et al.* 1994). The boundary-value problem (3.1), (3.4) is referred to as the radiation problem (RP).

The condition (3.4) is natural in the case when the source (3.2) decays sufficiently rapidly at large distances, as it eliminates waves ingoing from infinity. In this case the solution to the RP is unique (Sveshnikov *et al.* 2004, § VIII.6) and represented as a convolution of the source term with Green's function for the Helmholtz equation,

$$\rho_{11} = -\frac{\mathrm{i}}{4}\int_{\mathbb{R}^2} q_{11}(\boldsymbol{r}')H_0^{(1)}(|\boldsymbol{r}-\boldsymbol{r}'|)\,\mathrm{d}^2\boldsymbol{r}', \tag{3.6}$$

where $H_0^{(1)}(r)$ is the Hankel function of the first kind. The RP is well-posed if the integral in (3.6) converges absolutely and ill-posed otherwise, because a multiple integral converges only if it converges absolutely (Belyaev & Kopiev 2008). Using (3.2) and the asymptotics of the Hankel function

$$H_0^{(1)}(r) \sim \sqrt{\frac{2}{\pi r}}\exp(\mathrm{i}r - \mathrm{i}\pi/4) \quad \text{as } r \to \infty, \tag{3.7}$$

we come to the criterion for the well-posedness of the two-dimensional scattering problem in the Born approximation with the radiation condition

$$|q_{11}| = O(r^{-n}), \quad n > 3/2 \quad \text{as } r/R \to \infty, \tag{3.8}$$

or, without loss of generality,

$$|\boldsymbol{v}_{10}|\,|\boldsymbol{v}_{01}| = O(r^{-n}), \quad n > 3/2 \quad \text{as } r/R \to \infty, \tag{3.9}$$

where R is a suitable spatial scale. In the three-dimensional case we will have $n > 2$ instead of $n > 3/2$ in (3.8), (3.9).

When $|\boldsymbol{v}_{01}| = \text{const}$, the condition (3.9) is reduced to

$$|\boldsymbol{v}_{10}| = O(r^{-n}), \quad n > 3/2 \quad \text{as } r/R \to \infty. \tag{3.10}$$

The condition (3.10) is essentially different from the similar one obtained by Fabrikant (1983) for the vorticity $\nabla \times \boldsymbol{v}_{10}$ instead of the velocity $\boldsymbol{v}_{10}$. It follows that in case PWPV and, more broadly speaking, in the case of a uniform plane wave (1.3) scattering by an arbitrary flow with non-zero total circulation the RP is ill-posed. There is no contradiction because the total kinetic energy of an unbounded incompressible flow with $|\boldsymbol{v}_{10}| \propto r^{-1}$ as $r/R \to \infty$ is

$$E_{vort} \propto \frac{1}{2}\int_{\mathbb{R}^2} |\boldsymbol{v}_{10}|^2\,\mathrm{d}^2\boldsymbol{r} \propto \int^{\infty} \frac{\mathrm{d}r}{r} = \infty, \tag{3.11}$$

hence it cannot exist, as noted by Reinschke *et al.* (1997) and Gaifullin (2015, § III.1). In an unbounded three-dimensional fluid, only vortical structures with zero total circulation over any cross-section can emerge, such as the wake vortex behind an aeroplane with a high-aspect-ratio wing, which consists of two vortex tubes with opposite circulation, or the helicopter vortex ring. Examples for which the scattering problem is well-posed are given in § 1. As vortices with fractional power decay are unknown in fluid mechanics, in practice, condition (3.10) is equivalent to that of zero total circulation, i.e.

$$\Gamma \to 0 \quad \text{as } r/R \to \infty, \tag{3.12}$$

or, for a flow without singularities, that the total kinetic energy is finite.

However, for the case of $|\boldsymbol{v}_{01}| = \text{const}$ and a hypothetical vortex with $|\boldsymbol{v}_{10}| \propto r^{-3/2}$ as $r/R \to \infty$, the RP is ill-posed despite (3.12). There is no contradiction either because the total energy flux of a uniform plane wave is

$$W_{inc}(x) \propto \int_{-\infty}^{\infty} |\boldsymbol{v}_{01}|^2 \,\mathrm{d}y \propto \int_{-\infty}^{\infty} \mathrm{d}y = \infty, \tag{3.13}$$

hence it cannot exist. Here x, y are the Cartesian coordinates such that x is along the wave vector. The natural acoustic field with a finite total energy flux, emitted by a localised source in a two-dimensional fluid, is a cylindrical wave such as (1.4). In the case when it is an incident field, $|\boldsymbol{v}_{01}| \propto r^{-1/2}$ as $r/R \to \infty$, the condition (3.9) is reduced to (3.12). This shows that the scattering problem is well-posed for any physically sensible statement $E_{vort} < \infty$, $W_{inc} < \infty$. Meanwhile, there are unrealisable but still well-posed problems when (3.9) is fulfilled despite one of E_{vort}, W_{inc} being infinite. Examples with the exponential decay were proposed by Berthet & Lund (1995) (see § 1). However, the statement for a cylindrical incident wave and a vortex with non-zero circulation (1.6)–(1.7) proposed by Kopiev & Belyaev (2010) remains incorrect if considered in the Born approximation because $|\boldsymbol{v}_{10}||\boldsymbol{v}_{01}| \propto r^{-3/2}$ as $r/R \to \infty$.

4. Reformulation of the problem

Our purpose is the formulation of a well-posed RP for the case similar to case PWPV but with the appropriately confined region of the wave–vortex interaction. This means the specification of a source (3.2) that fulfills the condition (3.8). For compatibility with most of the existing works, we focus on a uniform plane wave (1.3) scattering by an axisymmetric vortex (1.6), similar to (1.7) within a limited region, but with a sufficiently rapidly decaying velocity field (3.10).

4.1. *Physics-based rationale*

The appropriate flow can be generated in a real fluid as follows. Let an infinitely elongated hollow solid circular cylinder of radius r_* be placed in a viscous fluid at rest, and at the moment $t = 0$ start to rotate around its axis with the constant angular velocity $\Gamma_*/2\pi r_*^2$. An unsteady axisymmetric vortex (1.6) arises owing to viscous friction. The leading-order solution to this problem for large t in the outside region $r > r_*$ in the framework of the compressible two-dimensional Navier–Stokes equations was obtained by Gadzhiev, Gaifullin & Zubtsov (2020). In the case of low Mach numbers $\Gamma_*/(r_* c_\infty) \ll 1$, the solution is reduced to one in an incompressible fluid. The flow is the difference between the irrotational vortex and the Lamb–Oseen (1912) vortex outside (Gaifullin 2015, § III.1), and a solid-body rotation inside. The circulation distribution is

$$\frac{\Gamma}{\Gamma_*} \sim \begin{cases} (r/r_*)^2, & r/r_* = O(1), \quad r \le r_* \\ 1, & r/r_* = O(1), \quad r > r_* \\ \exp(-r^2/(4\nu_\infty t)), & r/\sqrt{\nu_\infty t} = O(1) \end{cases} \quad \text{as } r_*/\sqrt{\nu_\infty t} \to 0, \tag{4.1}$$

where ν_∞ is kinematic viscosity of the unperturbed fluid. It can be considered as the Rankine vortex with circulation Γ_* screened by a vortical mantle with total circulation $-\Gamma_*$ expanding in time.

To organise the scattering problem, let us remove the cylinder at a sufficiently distant moment $t = t_0$ when the vortex effective radius $L = 2\sqrt{\nu_\infty t_0}$ is long compared with the

cylinder radius r_*, and let the uniform plane acoustic wave (1.3) start to propagate from the region $r \gg L$. The acoustic wavelength $\lambda = 2\pi/k$ is assumed much longer than r_* and much shorter than L. The Euler equations are valid as long as the viscous diffusion is negligible (see also Lund & Rojas 1989) so that the flow is approximately steady, for times $t - t_0 \ll r_*^2/\nu_\infty$. A time-periodic acoustic field is established in the whole relevant region $r/r_F = O(1)$ as soon as the incident wave has overcome it, for times $t - t_0 \gg r_F/c_\infty$. The longer the cylinder rotates, the larger is the region $r \ll L$ where (4.1) is reduced to the Rankine vortex lying within (1.7), which is the case PWPV. In the intermediate region $r_* < r \ll L$, the scattering pattern exists against an irrotational velocity field induced by the point vortex with intensity Γ_*.

4.1.1. *Validity of the formulation*

The physics-based rationale presented in § 4.1 uses the following assumptions: (i) the Mach numbers are small; (ii) there is a time interval for which the acoustic field is time-periodic in the relevant region wherein it reaches its far-field form (1.4); (iii) there is a region covering the wavelength scale where the velocity field is as induced by a point vortex. Condition (i) is ensured by (2.5). For condition (iii), we need

$$\delta = kr_* \ll 1, \quad \varepsilon = 1/(kL) \ll 1. \tag{4.2a,b}$$

For condition (ii), the incident wave has to overcome the region $r/r_F = O(1)$ long before time-periodicity is destroyed, which might be possible owing to: (*a*) the viscous diffusion of the vortex at times $O(r_*^2/\nu_\infty)$; (*b*) the acoustic instability of the Rankine vortex at $O(r_*^6 c_\infty^4/\Gamma_*^5)$ (see Kopiev & Leontiev (1983) and Kop'ev & Chernyshev (2000), § 3.2); (*c*) the nonlinear self-convection of the wave at $O(\omega^{-1}/a)$. Using the evaluation (5.9) we need to assume the following relationships between dimensional spatial scales:

$$\left.\begin{aligned} &\max\left(\nu_\infty/c_\infty,\ \Gamma_*/c_\infty\right) \ll r_* \ll \lambda \ll L \ll r_F = O(L^2/\lambda), \\ &L^2/\lambda \ll c_\infty(t - t_0) \ll \min\left(r_*^6 c_\infty^5/\Gamma_*^5,\ r_*^2 c_\infty/\nu_\infty,\ \lambda/a\right). \end{aligned}\right\} \tag{4.3}$$

In terms of dimensionless variables, the requirement that r_F/c_∞ is much shorter than the three temporal scales leads to additional restrictions for the small parameters (2.5), (4.2):

$$M^5 \ll \delta\varepsilon^2, \quad M \ll \mathrm{Re}\,\delta\varepsilon^2, \quad a \ll \varepsilon^2, \tag{4.4a–c}$$

where $\mathrm{Re} = \Gamma_*/\nu_\infty$. The first condition represents the restriction owing to instability, the second diffusion and the third nonlinear convection.

To apply perturbation theory, we also require the Born approximation (2.18). Equation (3.1) with the source (4.11), (4.10) suggests that the sufficient condition for its validity is high-frequency scattering, meaning that the angular frequency of the incident wave is high compared with the maximum angular velocity of the flow, i.e.

$$M/\delta = \Gamma_*/(2\pi\omega r_*^2) \ll 1. \tag{4.5}$$

The actual sufficient condition seems to be less rigorous than (4.5), though more rigorous than (2.5*b*):

$$M \ll \delta \quad \text{or} \quad M \ll 1, \quad M \neq \delta/n + O(\delta^2), \quad n \in \mathbb{Z}. \tag{4.6}$$

The latter restriction is related to fact that the Rankine vortex is able to emit sound on its eigenfrequencies nM/δ, where M/δ is the dimensionless angular velocity in the

region $r < \delta$. The same is likely for the case of the vortex (4.10), as it is similar to the Rankine vortex. When the angular frequency of the incident wave is close to one of the eigenfrequencies, the resonant amplification makes the scattered field comparable to the incident field (Sozou 1990; Ford & Smith 1999; Kopiev & Belyaev 2010).

4.2. *Mathematical formulation*

It is useful to redefine the dimensionless functions $\boldsymbol{U}_{ij}(\boldsymbol{r})$ by replacing the maximum flow Mach number $M = \Gamma_*/(2\pi r_* c_\infty)$ in the decomposition (2.6) with the Mach number at the acoustic wavelength scale $r = 1$ defined by

$$M_\lambda = M\delta = k\Gamma_*/(2\pi c_\infty). \tag{4.7}$$

In the Born approximation the leading-order scattered field satisfies the equations (3.1)–(3.3). The uniform plane incident wave (1.3*a*,*b*) that satisfies the linearised Euler equations is rewritten as

$$\rho_{01} = \exp(\mathrm{i}\hat{\boldsymbol{k}}\cdot\boldsymbol{r}), \quad p_{01} = \gamma\exp(\mathrm{i}\hat{\boldsymbol{k}}\cdot\boldsymbol{r}), \quad \boldsymbol{v}_{01} = \hat{\boldsymbol{k}}\exp(\mathrm{i}\hat{\boldsymbol{k}}\cdot\boldsymbol{r}), \tag{4.8a–c}$$

whereas the axisymmetric vortex (1.6*a*–*c*) is rewritten as

$$\rho_{10} = 0, \quad p_{10} = 0, \quad \boldsymbol{v}_{10} = \frac{\Gamma(r)}{r}\hat{\boldsymbol{\theta}}, \tag{4.9a–c}$$

where dimensionless circulation $\bar{\Gamma} = \Gamma/\Gamma_*$ (the overline is dropped hereafter) is defined by (4.1) and rewritten using (4.2) as

$$\Gamma \sim \begin{cases} (r/\delta)^2, & r/\delta = O(1), \quad r \le \delta \\ 1, & r/\delta = O(1), \quad r > \delta \\ \mathrm{e}^{-\varepsilon^2 r^2}, & \varepsilon r = O(1) \end{cases} \quad \text{as } \delta\varepsilon \to 0. \tag{4.10}$$

The subsequent approximations are not of interest, as they do not contribute to equations (3.1)–(3.3). The source (3.2), (4.8)–(4.9) is

$$q_{11} = -2\mathrm{i}\hat{\boldsymbol{k}}\cdot\nabla\left(\frac{\hat{\boldsymbol{z}}\cdot(\boldsymbol{r}\times\hat{\boldsymbol{k}})}{r^2}\Gamma(r)\exp(\mathrm{i}\hat{\boldsymbol{k}}\cdot\boldsymbol{r})\right), \tag{4.11}$$

where $\hat{\boldsymbol{z}} = \hat{\boldsymbol{r}}\times\hat{\boldsymbol{\theta}}$ is the unit vector along vorticity.

On condition (4.2), in the region of interest $r \gg 1$, the scattered field (3.6) for the source (4.11), (4.10) does not depend on δ in the leading-order approximation, i.e. the vorticity distribution over the vortex core is unimportant (see § 1). This enables us to take $\delta = 0$ as soon as we move to the RP, so that (4.10) is reduced to

$$\Gamma = \mathrm{e}^{-\varepsilon^2 r^2}. \tag{4.12}$$

The real part of the source (4.11), (4.12) for $\varepsilon = 0.05$ is presented in figure 3(*a*).

The RP for the source (4.11), (4.12) is the main point of the present work. The exponential decay

$$\Gamma = O((\varepsilon r)^{-\infty}) \quad \text{as } \varepsilon r \to \infty \tag{4.13}$$

ensures the problem is well posed for $\varepsilon > 0$. The substitution of $\varepsilon = 0$ into (4.12) leads to case PWPV with the point vortex $\Gamma = 1$, for which the problem is ill-posed. Our goal is the leading-order solution as $\varepsilon \to 0$ when there are two separate spatial scales

visible in figure 3(*a*): the acoustic wavelength $r = O(1)$ and the vortex effective radius $\varepsilon r = O(1)$. This does not require matched asymptotic expansions, as the exact solution (3.6) is known. The solution in the intermediate region $r \to \infty$, $\varepsilon r \to 0$, where the vortex is approximately irrotational so that

$$\Gamma \to 1 \quad \text{as } \varepsilon r \to 0, \tag{4.14}$$

as in case PWPV, is of particular interest. The model $\Gamma = \exp(-\varepsilon r)$ proposed by Berthet & Lund (1995), which also satisfies (4.13) and (4.14), is appropriate as well but has no clear physical background and seems to need more cumbersome calculations.

5. Leading-order solution as $\varepsilon \to 0$

5.1. *General representations*

5.1.1. *Representation using the Fourier transform*

First, it is useful to derive an exact representation of the solution to the general well-posed RP that does not contain non-elementary functions. Let us apply the two-dimensional Fourier transform

$$\widehat{\rho}_{11}(\boldsymbol{K}) = \frac{1}{2\pi}\int_{\mathbb{R}^2} \rho_{11}(\boldsymbol{r}) \exp(-\mathrm{i}\boldsymbol{K}\cdot\boldsymbol{r})\,\mathrm{d}^2\boldsymbol{r}, \quad \widehat{q}_{11}(\boldsymbol{K}) = \frac{1}{2\pi}\int_{\mathbb{R}^2} q_{11}(\boldsymbol{r}) \exp(-\mathrm{i}\boldsymbol{K}\cdot\boldsymbol{r})\,\mathrm{d}^2\boldsymbol{r} \tag{5.1a,b}$$

to the Helmholtz equation (3.1). Owing to the decay condition (3.5),

$$\frac{1}{2\pi}\int_{\mathbb{R}^2} \nabla^2\rho_{11} \exp(-\mathrm{i}\boldsymbol{K}\cdot\boldsymbol{r})\,\mathrm{d}^2\boldsymbol{r} = -K^2\widehat{\rho}_{11}. \tag{5.2}$$

Equations (5.1*a*,*b*) and (5.2) give

$$(1-K^2)\widehat{\rho}_{11} = \widehat{q}_{11}. \tag{5.3}$$

We extract $\widehat{\rho}_{11}$ and make the inverse Fourier transform, which gives

$$\rho_{11} = \frac{1}{2\pi}\int_{\mathcal{C}} \frac{\widehat{q}_{11}(\boldsymbol{K})}{1-K^2} \exp(\mathrm{i}\boldsymbol{K}\cdot\boldsymbol{r})\,\mathrm{d}^2\boldsymbol{K}. \tag{5.4}$$

The two-dimensional cycle $\mathcal{C} \subset \mathbb{C}^2$ in (5.4) is the plane $\mathbb{R}^2$ deformed to bypass the singular circle $K = 1$, which corresponds to eigensolutions of the Helmholtz operator, appropriately to fulfil the radiation condition (3.4)

$$\mathrm{Re}(\boldsymbol{K})\cdot\mathrm{Im}(\boldsymbol{K}) < 0 \quad \text{for } \boldsymbol{K} \in \mathcal{C} \text{ near } K = 1, \tag{5.5}$$

which is equivalent to the causality condition (see § 1). The representation (5.4) with $\mathcal{C}$ observing the rule of bypass (5.5) and the representation (3.6) are equivalent and related to each other by the convolution theorem.

5.1.2. *Far-field representation*

The source (4.11), (4.12) is localised within the flow region $\varepsilon r = O(1)$. Consequently, in the region of fluid at rest $\varepsilon r \to \infty$ it is possible to use asymptotics (3.7) for Green's function in (3.6), because any of the primitive waves emitted from the important region

$\varepsilon r' = O(1)$ overcome the long distance $|\boldsymbol{r} - \boldsymbol{r}'| \gg 1$. The distance is expanded in a power series by $\boldsymbol{r}'$ as

$$|\boldsymbol{r} - \boldsymbol{r}'| = r - \hat{\boldsymbol{r}} \cdot \boldsymbol{r}' + \frac{(\hat{\boldsymbol{\theta}} \cdot \boldsymbol{r}')^2}{2r} + O\left(\frac{1}{\varepsilon^3 r^2}\right) \quad \text{as } \varepsilon r \to \infty. \tag{5.6}$$

We need only keep the leading-order term of (5.6) in the denominator of (3.7), but the complete expansion in the exponent.

The greatest possible simplification for the exponent of (3.7) is the linearisation of (5.6) by $\boldsymbol{r}'$, known as the Fraunhofer approximation. It is valid only in the region $\varepsilon^2 r \to \infty$, the farthest part of the region of fluid at rest. Substituting this into (3.6) and using (3.3*b*), we obtain the outgoing cylindrical wave (1.4)

$$\rho_{11} \sim \frac{\exp(\mathrm{i}r - \mathrm{i}\pi/4)}{\sqrt{r}} f(\theta), \quad \boldsymbol{v}_{11} \sim \hat{\boldsymbol{r}}\rho_{11} \quad \text{as } \varepsilon^2 r \to \infty, \tag{5.7a,b}$$

with the scattering amplitude

$$f = -\mathrm{i}\sqrt{\frac{\pi}{2}}\widehat{q}_{11}(\hat{\boldsymbol{r}}), \tag{5.8}$$

where $\widehat{q}_{11}$ is the source Fourier transform defined by (5.1*b*). Its argument $\hat{\boldsymbol{r}}$ reflects the direction of sound propagation in the far field. The solution (5.7*a*), (5.8) satisfies the radiation condition (3.4) and in the leading-order approximation the Helmholtz equation (3.1), which is homogeneous because of (4.13). This can also be derived from (5.4) by using the multidimensional stationary-phase method (see Fedoryuk 1963).

In the region $\varepsilon^2 r = O(1)$ we need to keep the quadratic term of (5.6) dependent on $\boldsymbol{r}$, which leads to the breakdown of (5.7). This defines the bound of the far field according to (3.4) as

$$r_F = \varepsilon^{-2}. \tag{5.9}$$

Equation (5.9) indicates that the near field $r/r_F = O(1)$, where the scattered field is different from (5.7), is much longer than the flow region. This suggests a multiscale scattering pattern, including in the region of fluid at rest $\varepsilon r \to \infty$.

5.2. *Qualitative analysis*

The Fourier transform of the source (4.11), integrated by parts, is reduced to the Fourier transform of the longitudinal component of velocity (4.9*c*), with the argument shifted by the wave vector $\hat{\boldsymbol{k}}$ of incident wave (4.8), giving

$$\widehat{q}_{11}(\boldsymbol{K}) = \frac{1}{\pi}\boldsymbol{K} \cdot \hat{\boldsymbol{k}} \int_{\mathbb{R}^2} \frac{\hat{\boldsymbol{z}} \cdot (\boldsymbol{r} \times \hat{\boldsymbol{k}})}{r^2} \Gamma(r) \exp(-\mathrm{i}(\boldsymbol{K} - \hat{\boldsymbol{k}}) \cdot \boldsymbol{r})\, \mathrm{d}^2\boldsymbol{r}. \tag{5.10}$$

From the uncertainty principle, the Fourier transform (5.10) of the source (4.11), (4.12) distributed within the region $r = O(\varepsilon^{-1})$ is localised within the neighbourhood of the incident wave vector $|\boldsymbol{K} - \hat{\boldsymbol{k}}| = O(\varepsilon)$. This leads to considerable amplification of the scattered sound in the direction of incidence, because of the constructive interference between primitive waves, meaning that the instantaneous phase difference $\hat{\boldsymbol{k}} \cdot \boldsymbol{r}$ is neutralised by the path difference $-\boldsymbol{K} \cdot \boldsymbol{r}$. In particular, the far-field solution (5.8) is

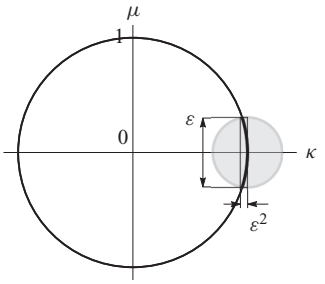

Figure 1. Asymptotic regions of the source Fourier transform $\widehat{q}_{11}(\boldsymbol{K})$ (filled circle) and the solution Fourier transform $\widehat{\rho}_{11}(\boldsymbol{K})$ as $\varepsilon \to 0$ presented in figure 3(*b*,*d*).

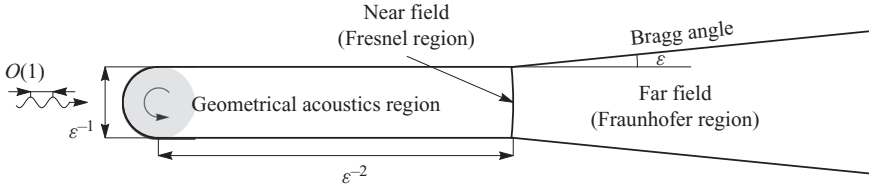

Figure 2. Asymptotic regions of the source $q_{11}(\boldsymbol{r})$ (filled circle) and the solution $\rho_{11}(\boldsymbol{r})$ as $\varepsilon \to 0$ presented in figure 3(*a*,*c*).

localised within, i.e. peaks at small scattering angles $|\hat{\boldsymbol{r}} - \hat{\boldsymbol{k}}| \sim \theta = O(\varepsilon)$. The Fourier transform of the exact solution (5.4) peaks at the part of the neighbourhood $|\boldsymbol{K} - \hat{\boldsymbol{k}}| = O(\varepsilon)$ with the incident wavenumber $K = 1$, where it is singular. This is the parabolic curve localised within the region $|\kappa - 1| = O(\varepsilon^2)$, $|\mu| = O(\varepsilon)$, where $\kappa = \hat{\boldsymbol{k}} \cdot \boldsymbol{K}$ and $\mu = \hat{\boldsymbol{z}} \cdot (\hat{\boldsymbol{k}} \times \boldsymbol{K})$ are Cartesian components of $\boldsymbol{K}$ (see figure 1). Owing to the uncertainty principle, the solution is distributed within the region $x = O(\varepsilon^{-2})$, $|y| = O(\varepsilon^{-1})$ oriented in the forward direction, where $x = \hat{\boldsymbol{k}} \cdot \boldsymbol{r} = r\cos\theta$ and $y = \hat{\boldsymbol{z}} \cdot (\hat{\boldsymbol{k}} \times \boldsymbol{r}) = r\sin\theta$ are Cartesian coordinates. This suggests an outgoing cylindrical wave (5.7) beyond, and a different solution within, this region. Thus, in the case of a plane incident wave (4.8) the near field holds the flow region $r = O(\varepsilon^{-1})$ and the wake of length $O(\varepsilon^{-2})$ behind it (see figure 2); the remaining part degenerates into the far field, so that the bound (5.9) is constricted to

$$r_F(\theta) = \begin{cases} \varepsilon^{-2}, & \theta/\varepsilon = O(1) \\ \varepsilon^{-1}/\theta, & \theta/\varepsilon \to \infty, \end{cases} \tag{5.11}$$

maintained at small angles. Note that figure 2, as well as figure 6, implies a homomorphism that maps the relationship 'much less than' to 'less than' and 'similar to' to 'approximately equal to', so values of the same order are shown as identical. In particular, the regions $\varepsilon^2 r \to \infty$ and $\varepsilon^2 r \to 0$ correspond to areas, while the region $\varepsilon^2 r = O(1)$ excluding $\varepsilon^2 r \to 0$ to a curve.

Overall, there is a profound analogy between the scattering pattern in the present problem and the diffraction pattern in the problem of a plane wave short-wavelength diffraction by a slit when the wavelength is of $O(1)$ whereas the slit width is of $O(\varepsilon^{-1})$. A thorough description was provided by Tatarski (2016, § 2), Monin & Yaglom (2013, § 26) who considered the plane wave scattering by a limited volume of turbulence. Berthet *et al.* (2003) noted this for the case close to case PWPV, yet with the vorticity localised within a region long compared with the acoustic wavelength. The cause is the analogy

between the representation (3.6) and two-dimensional Kirchhoff's diffraction formula (see Schot (1992) and Krylov (1989), S 3), both of which are based on the Helmholtz equation (3.1), though a source is distributed for scattering by a flow and localised on a one-dimensional surface for diffraction by an aperture. On the forward direction, where the diffraction pattern is typically of interest, the far field $\varepsilon^2 r \to \infty$ can be identified with the Fraunhofer region, while the near field $\varepsilon^2 r = O(1)$ with the Fresnel region. The angular region $\theta/\varepsilon = O(1)$ is the same as that specified by Bragg's law (Kambe & Oo 1981). The subregion $\varepsilon^2 r \to 0$ of the near field is accordingly interpreted as the region of geometrical (ray) acoustics where the acoustic wavelength does not matter, i.e. the wave propagates as a beam of rays. However, Nazarenko *et al.* (1995) noted that the Born approximation and the geometrical acoustics approach developed by Lindsay (1948), Salant (1969), Nazarenko (1994) and Nazarenko *et al.* (1995) for case PWPV have no common limit, which prevents comparison with their results.

5.3. *Solution for the case* $\Gamma = \exp(-\varepsilon^2 r^2)$

The Fourier transform of the source (4.11), (4.12) is calculated with a relationship that can be derived using the convolution theorem and was used by Candel (1979), who considered case PWPV for the Lamb–Oseen vortex, namely,

$$\frac{1}{2\pi}\int_{\mathbb{R}^2} \frac{\hat{\boldsymbol{z}}\cdot(\boldsymbol{r}\times\hat{\boldsymbol{k}})}{r^2}\exp(-\varepsilon^2 r^2)\exp(-\mathrm{i}\boldsymbol{\alpha}\cdot\boldsymbol{r})\,\mathrm{d}^2\boldsymbol{r} = -\mathrm{i}\frac{\hat{\boldsymbol{z}}\cdot(\boldsymbol{\alpha}\times\hat{\boldsymbol{k}})}{\alpha^2}(1-\exp(-\alpha^2/4\varepsilon^2)). \tag{5.12}$$

Substituting (5.12) into (5.10), (4.12) we obtain

$$\widehat{q}_{11}(\boldsymbol{K}) = -2\mathrm{i}\frac{\boldsymbol{K}\cdot\hat{\boldsymbol{k}}\,\hat{\boldsymbol{z}}\cdot(\boldsymbol{K}\times\hat{\boldsymbol{k}})}{|\boldsymbol{K}-\hat{\boldsymbol{k}}|^2}(1-\exp(-|\boldsymbol{K}-\hat{\boldsymbol{k}}|^2/4\varepsilon^2)). \tag{5.13}$$

The imaginary parts of the source Fourier transform (5.13) and of the solution Fourier transform (5.13)/$(1-K^2)$ for $\varepsilon = 0.05$ are presented in figures 3(*b*) and 3(*d*), respectively (compare with the scheme in figure 1).

The complete calculations carried out using the exact representation (5.4) with the bypass rule (5.5) for the source Fourier transform (5.13) are presented in Appendix A. All the plots throughout this paper are for the value $\varepsilon = 0.05$. The real part of the solution obtained by numerical integration of the single integral (A1), (A4)–(A10) is presented in figure 3(*c*) (compare with the scheme in figure 2). The leading-order analytical solution is present in the far field $\varepsilon^2 r \to \infty$, at large angles $\theta/\varepsilon \to \infty$ and in the region of geometrical acoustics $\varepsilon^2 r \to 0$. The condition $r \to \infty$ is always assumed and is dropped hereafter.

5.3.1. *Far field* $\varepsilon^2 r \to \infty$

The scattering amplitude in the far field can be obtained by direct substitution of (5.13) into (5.8) giving

$$f = f^{(i)}(1-\exp(-|\hat{\boldsymbol{r}}-\hat{\boldsymbol{k}}|^2/4\varepsilon^2)) \sim f^{(i)}(1-\exp(-\theta^2/4\varepsilon^2)), \tag{5.14}$$

where

$$f^{(i)} = -\sqrt{2\pi}\,\frac{\hat{\boldsymbol{r}}\cdot\hat{\boldsymbol{k}}\,\hat{\boldsymbol{z}}\cdot(\hat{\boldsymbol{r}}\times\hat{\boldsymbol{k}})}{|\hat{\boldsymbol{r}}-\hat{\boldsymbol{k}}|^2} = \sqrt{\frac{\pi}{2}}\cos\theta\cot\frac{\theta}{2} \tag{5.15}$$

is exactly expression (i) with the singularity for case PWPV, $|\hat{\boldsymbol{r}}-\hat{\boldsymbol{k}}| = 2\sin(\theta/2)$.

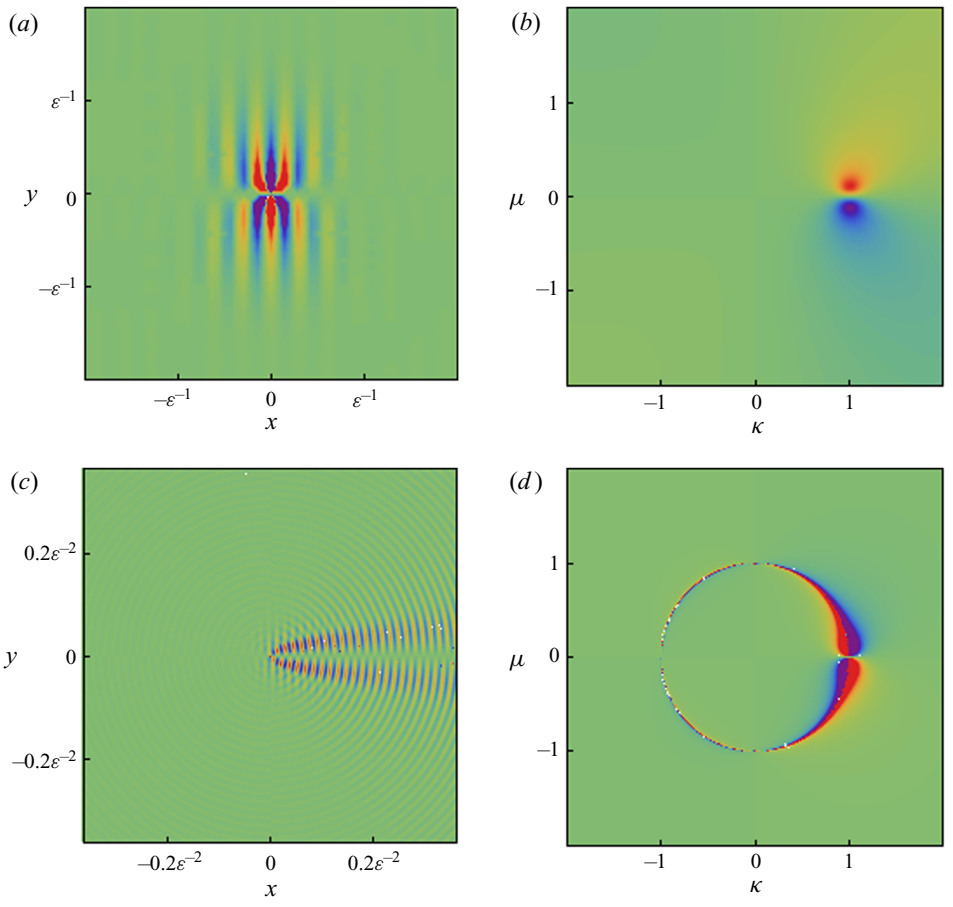

Figure 3. The source $\mathrm{Re}(q_{11})$ (4.11) (*a*) and its Fourier transform $\mathrm{Im}(\widehat{q}_{11})$ (5.13) (*b*), the solution $\mathrm{Re}(\rho_{11})$ (A1), (A4)–(A10) (*c*) and its Fourier transform $\mathrm{Im}(\widehat{\rho}_{11})$ (5.13)/$(1-K^2)$ (*d*) for $\Gamma(r)=\exp(-\varepsilon^2 r^2)$, $\varepsilon=0.05$. The ranges displayed are $-0.2<\mathrm{Re}(q_{11})<0.2$, $-\varepsilon^{-1}<\mathrm{Im}(\widehat{q}_{11})<\varepsilon^{-1}$, $-2.62<\mathrm{Re}(\rho_{11})<2.62$ and $-2\varepsilon^{-1}<\mathrm{Im}(\widehat{\rho}_{11})<2\varepsilon^{-1}$.

By the analogous method Berthet & Lund (1995) obtained the solution for the case $\Gamma=\exp(-\varepsilon r)$

$$f=f^{(i)}\frac{|\hat{\boldsymbol{r}}-\hat{\boldsymbol{k}}|^2/\varepsilon^2}{\sqrt{1+|\hat{\boldsymbol{r}}-\hat{\boldsymbol{k}}|^2/\varepsilon^2}\left(1+\sqrt{1+|\hat{\boldsymbol{r}}-\hat{\boldsymbol{k}}|^2/\varepsilon^2}\right)}, \tag{5.16}$$

with the possible substitution $|\hat{\boldsymbol{r}}-\hat{\boldsymbol{k}}|\to\theta$ as in (5.14). However, there was no clear definition of the far field $\varepsilon^2 r\to\infty$ where (5.16) was valid. Its application to the region that is actually the near field is incorrect and, in particular, leads to a violation of the Helmholtz equation (3.1) in the flow region (see the explanation in § 5.4).

Both (5.14) and (5.16) are regular patterns that peak at small scattering angles so that

$$f=O(\varepsilon^{-1}),\quad |\boldsymbol{U}_{11}|=O(\varepsilon^{-1}/\sqrt{r})\ll 1\quad \text{as } \theta/\varepsilon=O(1), \tag{5.17a,b}$$

$$f=O(1),\quad |\boldsymbol{U}_{11}|=O(1/\sqrt{r})\quad \text{as } \theta=O(1), \tag{5.18a,b}$$

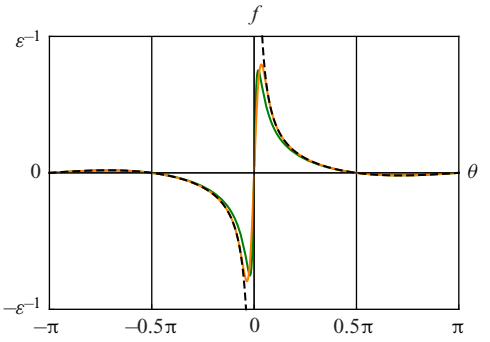

Figure 4. The scattering amplitude in the far field: expression (i) (5.15) for $\Gamma = 1$ (black, dashed); the solution (5.14) for $\Gamma = \exp(-\varepsilon^2 r^2)$, $\varepsilon = 0.05$ (orange, solid); the solution (5.16) for $\Gamma = \exp(-\varepsilon r)$, $\varepsilon = 0.05$ (dark green, solid).

and match expression (i) at large angles (figure 4), i.e.

$$f \sim f^{(i)} \quad \text{as } \theta/\varepsilon \to \infty. \tag{5.19}$$

5.3.2. *Region of geometrical acoustics* $\varepsilon^2 r \to 0$

The scattered field in the region of geometrical acoustics includes both the radiation component and the distortion component defined in § 2.1, i.e.

$$\boldsymbol{U}_{11} = \boldsymbol{U}^r_{11} + \boldsymbol{U}^d_{11}. \tag{5.20}$$

We remember that in the far field only the radiation component is present, meaning that $\boldsymbol{U}^d_{11} \to 0$ as $\varepsilon^2 r \to \infty$. We will use the fact that the amplitude and phase (2.21*a*,*b*) of a uniform plane incident wave (4.8) are, respectively,

$$A_0 = 1, \quad \varphi_0 = \hat{\boldsymbol{k}} \cdot \boldsymbol{r}, \tag{5.21a,b}$$

whereas the amplitude change and phase shift (2.22*a*,*b*) owing to scattering are given by

$$A_1 = |\rho_{11}| \cos(\arg \rho_{11} - \hat{\boldsymbol{k}} \cdot \boldsymbol{r}), \quad \varphi_1 = |\rho_{11}| \sin(\arg \rho_{11} - \hat{\boldsymbol{k}} \cdot \boldsymbol{r}). \tag{5.22a,b}$$

The radiation component is

$$\left.\begin{aligned} \rho^r_{11} &\sim -\pi \mathrm{i} \exp(\mathrm{i}r(1-\theta^2/2)) \frac{\theta}{2} \cos\theta \cot\frac{\theta}{2} \left[\operatorname{sgn}(\theta) - \operatorname{erf}\left(\frac{\mathrm{e}^{-\mathrm{i}\pi/4}\sqrt{r}\theta}{\sqrt{2}} \right) \right], \\ \boldsymbol{v}^r_{11} &\sim \hat{\boldsymbol{r}} \rho^r_{11}. \end{aligned}\right\} \tag{5.23}$$

Within the narrow parabolic region at small angles, it represents the non-decaying field with

$$|\boldsymbol{U}^r_{11}| = O(1) \quad \text{as } \sqrt{r}\theta = O(1). \tag{5.24}$$

At large angles, (5.23) as well as the far-field solution (5.14) is the outgoing cylindrical wave matching expression (i):

$$\rho^r_{11} \sim \frac{\exp(\mathrm{i}r - \mathrm{i}\pi/4)}{\sqrt{r}} f^{(i)}(\theta) \quad \text{as } \sqrt{r}\theta \to \infty. \tag{5.25}$$

The angular ranges of (5.14) and (5.23) are different, each being extrapolated to another region will be narrow compared with its counterpart (see figure 6).

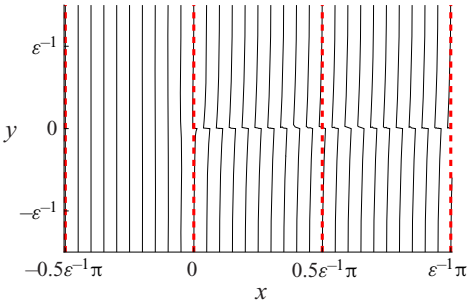

Figure 5. The wavefronts of the incident field defined by (4.8) $x = -10\pi; 0; 10\pi; 20\pi$ (red, dashed) and by (5.26), (5.27*b*), (5.28) $x + M_\lambda \varphi_1^d = \pi n$, $n \in \mathbb{Z}$ (black, solid) in the region of geometrical acoustics $\varepsilon^2 r \to 0$ for $\Gamma = \exp(-\varepsilon^2 r^2)$, $\varepsilon = 0.05$ and $M_\lambda = 0.25$.

The distortion component is

$$\begin{aligned}\rho_{11}^d &\sim -\mathrm{i}\exp(\mathrm{i}\hat{\boldsymbol{k}}\cdot\boldsymbol{r})\int_{-\hat{\boldsymbol{k}}\infty}^{\boldsymbol{r}} \hat{\boldsymbol{k}}\cdot\boldsymbol{v}_{10}(\boldsymbol{r}')\hat{\boldsymbol{k}}\cdot\mathrm{d}\boldsymbol{r}' \\ &= \pi\mathrm{i}\,\mathrm{e}^{\mathrm{i}x}\left[2T\left(\sqrt{2}\varepsilon y, x/y\right) + \frac{1}{2}(\operatorname{sgn}(y) - \operatorname{erf}(\varepsilon y))\right], \\ \boldsymbol{v}_{11}^d &\sim \hat{\boldsymbol{k}}\rho_{11}^d,\end{aligned} \tag{5.26}$$

where the Owen T-function is defined by (A5). It represents a non-uniform plane wave that does not interfere with the incident wave (4.8), giving

$$A_1^d = 0, \quad \varphi_1^d = \operatorname{sgn}(y)|\rho_{11}^d|, \tag{5.27a,b}$$

as follows from (5.22*a*,*b*). In terms of the alternative definition (2.28), (2.30), the scattered wave corresponds to (5.23), whereas the incident wave corresponds to (4.8*a*,*c*) $+M_\lambda$ (5.26). The latter is a non-uniform plane wave that can be rewritten using (5.21) as

$$\rho'_{inc} \propto \rho_{01} + M_\lambda \rho_{11}^d \sim \exp[\mathrm{i}(\hat{\boldsymbol{k}}\cdot\boldsymbol{r} + M_\lambda \varphi_1^d(\boldsymbol{r}))]. \tag{5.28}$$

The wavefront of (5.28) is retarded in the half-plane $y > 0$, where sound propagates upstream, and advanced in $y < 0$, where sound propagates downstream (figure 5). According to the integral expression in (5.26), the phase shift (5.27*b*) is proportional to the circulation of the vortex velocity along the straight line from the infinity inlet. Wavefront distortion is localised within the flow region and in the wake behind it such that

$$|\boldsymbol{U}_{11}^d| = O(1) \quad \text{as } \varepsilon r\theta = O(1), \tag{5.29}$$

and decays exponentially beyond. In the region of fluid at rest where $\Gamma \to 0$, from (5.26) we have

$$\rho_{11}^d \sim \pi\mathrm{i}\,\mathrm{e}^{\mathrm{i}x}\mathcal{H}(x)[\operatorname{sgn}(y) - \operatorname{erf}(\varepsilon y)] \quad \text{as } \varepsilon r \to \infty, \tag{5.30}$$

where $\mathcal{H}(x)$ is the Heaviside step function, equal to 1 in the forward direction and 0 in the backward direction. In the region $\varepsilon y \to 0$, which includes the irrotational flow region

$\varepsilon r \to 0$ where $\Gamma \to 1$,

$$\rho_{11}^{d} \sim \pi \mathrm{i} \exp(\mathrm{i}r\cos\theta)[\mathrm{sgn}(\theta) - \theta/\pi] \quad \text{as } \varepsilon y \to 0. \tag{5.31}$$

According to (5.31) the wavefront distortion owing to the velocity field decaying proportional to r^{-1} as $r \to \infty$ is finite, because the longitudinal velocity is proportional to x^{-2} as $x \to \infty$ (see McIntyre (2019), figure 2).

To summarise, the scattered field (5.23) + (5.26) beyond the flow region and the wake is the outgoing cylindrical wave matching expression (i),

$$\rho_{11} \sim \frac{\exp(\mathrm{i}r - \mathrm{i}\pi/4)}{\sqrt{r}} f^{(i)}(\theta), \quad \boldsymbol{v}_{11} \sim \hat{\boldsymbol{r}}\rho_{11} \quad \text{as } \varepsilon r\theta \to \infty. \tag{5.32a,b}$$

This confirms the suggestion of §5.2 that this region is, in fact, the far field. As the wake in (5.26) is wide compared with the parabolic region in (5.23) (see figure 6), in the intermediate region the distortion component dominates such that

$$\rho_{11} \sim \rho_{11}^{d}, \quad \boldsymbol{v}_{11} \sim \hat{\boldsymbol{k}}\rho_{11} \quad \text{as } \varepsilon r\theta = O(1). \tag{5.33a,b}$$

However, only the radiation component contributes to the interference pattern, so that

$$|\boldsymbol{U}_{11}| = O(1), \quad |A_1| = O(1/\sqrt{r}) \quad \text{as } \varepsilon r\theta = O(1). \tag{5.34a,b}$$

Within the parabolic region

$$|\boldsymbol{U}_{11}| = O(1), \quad |A_1| = O(1) \quad \text{as } \sqrt{r}\theta = O(1). \tag{5.35a,b}$$

The discontinuity in the direction $\theta = 0$, which is present in (5.23) as well as in (5.26), vanishes on summation.

The solution (5.23) + (5.31) is precisely expression (ii) for the case PWPV $\Gamma = 1$ that does not decay anywhere. (The corresponding scattered field in terms of the definition (2.30) does not decay only within the parabolic region $\sqrt{r}\theta = O(1)$.) It is valid in the irrotational flow region $\varepsilon r \to 0$ where $\Gamma \to 1$. Moreover, it persists in the region $\varepsilon^2 x \to 0$, $\varepsilon y \to 0$ including its backward as well as forward part, meaning that the scattered wave does not feel the decay of the flow. Independence of the solution on ε indicates the region of geometrical acoustics, since the wavelength remains the only spatial scale. Expression (ii) was obtained in equivalent forms by Aharonov & Bohm (1959, (21) and (23)), Berry *et al.* (1980, (14) and (A9)), Sakov (1993, (23)), Ford & Smith (1999, (5.7) and (5.11)–(5.12)), Howe (1999, (6), (11), (12), (14) and (17)) and Kopiev & Belyaev (2010, (21), (24), (32) and (34)), some of which were related to different variables and some contained misprints.

5.3.3. *Near field* $\varepsilon^2 r = O(1)$

The near-field solution at large angles, consistent with the foregoing is the outgoing cylindrical wave matching expression (i), written

$$\rho_{11} \sim \frac{\exp(\mathrm{i}r - \mathrm{i}\pi/4)}{\sqrt{r}} f^{(i)}(\theta) \quad \text{as } \varepsilon^2 r = O(1), \quad \theta/\varepsilon \to \infty. \tag{5.36}$$

The solution in the near field $\varepsilon^2 r = O(1)$ at small angles $\theta/\varepsilon = O(1)$ is obtained only as the single integral (A1), (A4)–(A10) and cannot be unambiguously divided into the radiation and distortion components. Some researchers who used the terminology of

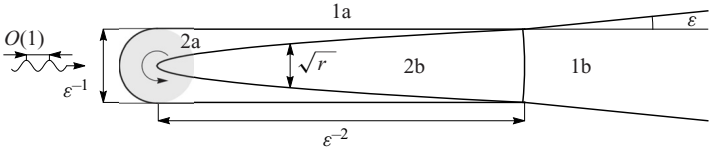

Figure 6. Asymptotic regions of the source (filled circle) and the solution presented in figure 10 as $\varepsilon \to 0$ in terms of orders of quantities corresponding to table 1.

	$\sqrt{r}\lvert A_1\rvert = O(1)$	$\sqrt{r}\lvert A_1\rvert \gg 1$
Far field:	1a	1b
$\lvert U_{11}\rvert \ll 1$	$\lvert U_{11}\rvert = O(1/\sqrt{r})$ $\lvert A_1\rvert = O(1/\sqrt{r})$ $\lvert f\rvert = O(1)$	$\lvert U_{11}\rvert = O(\varepsilon^{-1}/\sqrt{r})$ $\lvert A_1\rvert = O(\varepsilon^{-1}/\sqrt{r})$ $\lvert f\rvert = O(\varepsilon^{-1})$
Near field:	2a	2b
$\lvert U_{11}\rvert = O(1)$	$\lvert U_{11}\rvert = O(1)$ $\lvert A_1\rvert = O(1/\sqrt{r})$ $\lvert f\rvert = O(\sqrt{r})$	$\lvert U_{11}\rvert = O(1)$ $\lvert A_1\rvert = O(1)$ $\lvert f\rvert = O(\sqrt{r})$

Table 1. Orders of $|U_{11}|$, $|A_1|$, $|f|$ in asymptotic regions shown in figure 6.

(2.28), (2.30) interpreted that the incident and scattered fields could not be separated from each other. Here, the scattered field is rearranged from (5.23) + (5.26) in the region of geometrical acoustics to qualitatively different (5.7*a*,*b*), (5.14), (5.15) in the far field. The order of the amplitude is evidently

$$|U_{11}| = O(1) \quad \text{as } \varepsilon^2 r = O(1), \quad \theta/\varepsilon = O(1). \tag{5.37}$$

5.3.4. *Overall pattern*

The evaluations in §§ 5.3.1–5.3.3 define four asymptotic regions with different orders of $|U_{11}|$, $|A_1|$, which can be classified by two independent criteria (figure 6 and table 1). The region of geometrical acoustics is included in the near field in this sense. The far field 1a ∪ 1b and the near field 2a ∪ 2b are exactly the regions predicted by the analysis of the Fourier representation in § 5.2 (compare with figure 2). In addition, the far field and the near field are exactly the regions where the amplitude of the scattered wave $|U_{11}| \ll 1$ and $|U_{11}| = O(1)$, respectively. Note that $\max |U_{11}| = O(1)$, so that the Born approximation remains uniformly valid as required.

The solution obtained is reduced to expressions (i) and (ii) for case PWPV $\Gamma = 1$ and an analogue to the solution by Berthet & Lund (1995) for the case $\Gamma = \exp(-\varepsilon r)$ in different regions (table 2).

The real part of the numerical solution obtained using the exact representation (A1), (A4)–(A10) is presented in figure 3(*c*). In order to visualise the near-field solution in a similar manner to the far-field, it is useful to generalise the scattering amplitude to the complex-valued function dependent on r by

$$\rho_{11} \equiv \frac{\exp(\mathrm{i}r - \mathrm{i}\pi/4)}{\sqrt{r}} f(\boldsymbol{r}). \tag{5.38}$$

Scattering patterns $|f(r, \theta)|$ on various distances $r = \text{const}$ within the region of fluid at rest $\varepsilon r \gg 1$ are presented in figures 7–9, including the leading-order solution as $\varepsilon \to 0$

	Expression (i)	Expression (ii)	Solution by Berthet & Lund (1995)
Equation	(5.7), (5.49), (5.15)	(5.23) + (5.31)	(5.7), (5.16), (5.15)
Properties:			
regularity	−	+	+
decay at ∞	+	−	+
Case	$\Gamma = 1$	$\Gamma = 1$	$\Gamma = \exp(-\varepsilon r)$
Well-posedness of problem	ill-posed	ill-posed	well-posed
First obtained:			
exactly	Pitaevskii (1959)	Sakov (1993)	
analogous		Aharonov & Bohm (1959)	Berthet & Lund (1995)
Corresponding region	far field, large angles 1a	geom. acoustics region (near field 2a ∪ 2b, 'inner' part)	far field 1a ∪ 1b

Table 2. Known expressions that are included in the present solution in different regions (see figure 6).

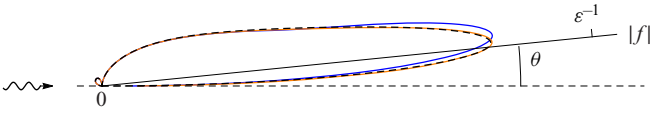

Figure 7. Scattering patterns in the far field for $\Gamma = \exp(-\varepsilon^2 r^2)$, $\varepsilon = 0.05$: the leading-order solution as $\varepsilon^2 r \to \infty$ (5.14) (black, dashed) and the numerical solution for $\varepsilon^2 r = 0.5$ (blue, solid) and $\varepsilon^2 r = 1$ (orange, solid).

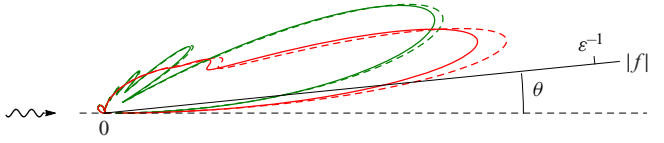

Figure 8. Scattering patterns in the region of geometrical acoustics for $\Gamma = \exp(-\varepsilon^2 r^2)$, $\varepsilon = 0.05$: the leading-order solution for $\varepsilon r \to \infty$, $\varepsilon^2 r \to 0$ corresponding to (5.23) + (5.30) (dashed) and the numerical solution (solid) for $\varepsilon r = 2$, $\varepsilon^2 r = 0.1$ (dark green), $\varepsilon r = 4$, $\varepsilon^2 r = 0.2$ (red).

determined in §§ 5.3.1 and 5.3.2 and the numerical solution. As $f(r, -\theta) = -f(r, \theta)$, only the upper half-plane $0 \le \theta \le \pi$ is shown. Peaks at small angles and nulls in the forward $\theta = 0$, transverse $\theta = \pi/2$ and backward $\theta = \pi$ directions are visible. Figure 9(*a*,*c*) shows that in practice the region $r < 0.2\varepsilon^{-2}$ can be considered as the region of geometrical acoustics, whereas the region $r > 0.5\varepsilon^{-2}$ can be considered as the far field. The oscillations appearing in the region of geometrical acoustics (figure 8) reflect the interference of the radiation component (5.23) and the distortion component (5.26).

The real part of the total acoustic field $\rho_{01} + M_\lambda \rho_{11}$ calculated using (4.8*a*) and (A1), (A4)–(A10) for $M_\lambda = 0.5$ (for a clear illustration) is presented in figure 10 (compare with the scheme in figure 6). The sharpest interference pattern $|A_1| = O(1)$ occurs in the parabolic region 2b. The most considerable wavefront refraction is visible in the near field 2a ∪ 2b. In the region 2a the wavefronts are similar to those shown in figure 5 (adjusted for the value of M_λ), while in the region 2b the gap is smoothed out. Similar behaviour can be observed in a physical or numerical experiment if the vortex velocity field exists in a

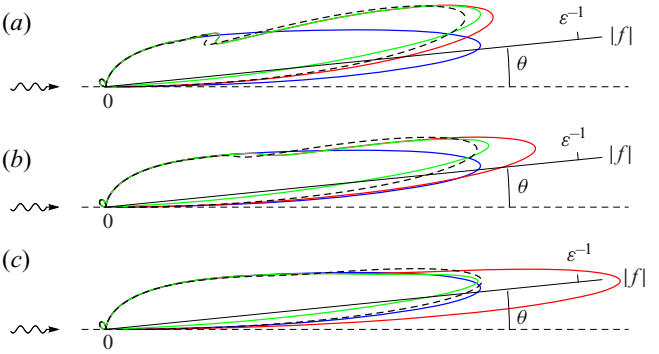

Figure 9. Scattering patterns for $\Gamma = \exp(-\varepsilon^2 r^2)$, $\varepsilon = 0.05$: the leading-order solution in the far field (5.14) (blue, solid), the leading-order solution in the region of geometrical acoustics corresponding to (5.23) + (5.30) (red, solid), the composite solution corresponding to (5.39) (green, solid) and the numerical solution (black, dashed) for $\varepsilon^2 r = 0.2$ (*a*); $\varepsilon^2 r = 0.3$ (*b*); $\varepsilon^2 r = 0.5$ (*c*).

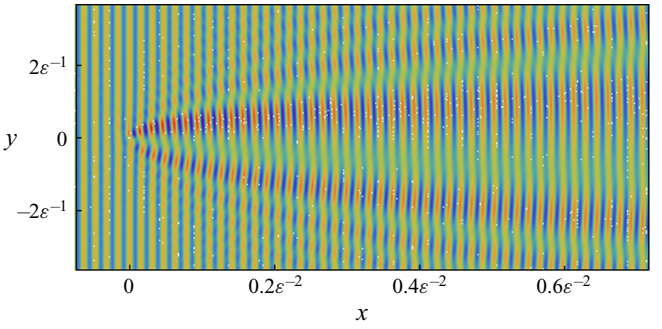

Figure 10. The total acoustic field $\mathrm{Re}(\rho_{01} + M_\lambda \rho_{11})$ given by (4.8*a*) + M_λ (A1), (A4)–(A10) for $\Gamma = \exp(-\varepsilon^2 r^2)$, $\varepsilon = 0.05$ and $M_\lambda = 0.5$.

limited region. Examples are water waves patterns corresponding to the cases of small M_λ (Vivanco *et al.* 1999, figure 2*a*,*b*) and numerical patterns (Berthet & Coste 2003, figures 6, 7). Compare it with results by Berry *et al.* (1980, figures 3, 4) for case PWPV and by Coste *et al.* (1999, figures 2*a*, 3*a*) for a similar case in which the refraction was considerable at arbitrarily large distances.

The structure of the solution allows us to compose a single expression that will be uniformly valid in the far field $\varepsilon^2 r \to \infty$, at large angles $\theta/\varepsilon \to \infty$ and in the region of geometrical acoustics $\varepsilon^2 r \to 0$. For this we use the technique analogous to the method of multiplicative composition, which is commonly used to obtain a uniformly valid solution from matched asymptotic expansions by taking the multiplication of the outer and inner expansions divided by the intermediate approximation (Van Dyke 1964, § 5.10). Let us regard the far-field solution (5.7*a*), (5.14), (5.15) as the outer expansion, the solution in the region of geometrical acoustics (5.23) + (5.26) as the inner expansion and the solution at large angles (5.36), (5.15) as the intermediate approximation. This is possible because in

the region 1a the expansions match each other. The composite solution is

$$\frac{\rho_{11}|_{\varepsilon^2 r\to\infty}\rho_{11}|_{\varepsilon^2 r\to 0}}{\rho_{11}|_{\theta/\varepsilon\to\infty}} \sim \pi\mathrm{i}(1-\exp(-\theta^2/4\varepsilon^2))$$
$$\times\left\{\exp(\mathrm{i}r\cos\theta)\left[2T(\sqrt{2}\varepsilon r\sin\theta,\cot\theta)+\frac{1}{2}\left(\mathrm{sgn}(\theta)-\mathrm{erf}(\varepsilon r\sin\theta)\right)\right]\right.$$
$$\left.-\exp(\mathrm{i}r(1-\theta^2/2))\frac{\theta}{2}\cos\theta\cot\frac{\theta}{2}\left[\mathrm{sgn}(\theta)-\mathrm{erf}\left(\frac{\mathrm{e}^{-\mathrm{i}\pi/4}\sqrt{r}\theta}{\sqrt{2}}\right)\right]\right\}. \tag{5.39}$$

The expression (5.39) looks more similar to the numerical solution than any of the known leading-order solutions, including in the near field (figure 9*b*). Apart from the near field, the only region where it leads to the relative error $O(1)$ is the non-relevant neighbourhood of the symmetry axis, where $\rho_{11}\propto\theta$ whereas (5.39) is proportional to θ^3.

5.3.5. *Scattering and momentum-transfer cross-sections*

Let us generalise the total scattering cross-section and momentum-transfer cross-section (Pitaevskii 1959) by taking into account the direction of the scattered-wave propagation. In the dimensionless form

$$\sigma(r)=\int_{-\pi}^{\pi}|\boldsymbol{v}_{11}|^2\hat{\boldsymbol{v}}_{11}\cdot\boldsymbol{r}\,\mathrm{d}\theta,\quad \sigma^*(r)=\int_{-\pi}^{\pi}|\boldsymbol{v}_{11}|^2(\hat{\boldsymbol{v}}_{11}-\hat{\boldsymbol{k}})\cdot\boldsymbol{r}\,\mathrm{d}\theta, \tag{5.40a,b}$$

where $\hat{\boldsymbol{v}}_{11}=\boldsymbol{v}_{11}/|\boldsymbol{v}_{11}|$ is the scattered wave vector, $\hat{\boldsymbol{v}}_{11}\to\hat{\boldsymbol{r}}$ as $\varepsilon^2 r\to\infty$. In the region of fluid at rest where the wave–vortex interaction is negligible, the scattered energy flux and momentum transfer must be constant,

$$\sigma(r)\to\sigma_\infty,\quad \sigma^*(r)\to\sigma^*_\infty\quad \text{as } \varepsilon r\to\infty. \tag{5.41a,b}$$

The far-field representation (5.7*a*,*b*) substituted into (5.40*a*,*b*) leads to

$$\sigma_\infty=\int_{-\pi}^{\pi}f^2(\theta)\,\mathrm{d}\theta,\quad \sigma^*_\infty=\int_{-\pi}^{\pi}f^2(\theta)(1-\cos\theta)\,\mathrm{d}\theta. \tag{5.42a,b}$$

For the solution (5.14), the total scattering cross-section (5.42*a*) is

$$\sigma_\infty\to 4\pi\int_0^\infty\frac{(1-\exp(-\theta^2/4\varepsilon^2))^2}{\theta^2}\mathrm{d}\theta=(4-2\sqrt{2})\pi^{3/2}\varepsilon^{-1}. \tag{5.43}$$

It is comparable to the size of the flow region, with most of the energy being emitted within small angles $\theta/\varepsilon=O(1)$. The dimensional total scattering cross-section is $O(M^2\delta^2\varepsilon^{-1})$ relative to the wavelength, this can be either longer or shorter as it is not limited by the conditions (4.4*a*–*c*).

In the region of geometrical acoustics beyond the flow region, substituting (5.23) + (5.30) into (5.40*a*) we obtain

$$\sigma\to 2\pi^2 r\int_0^\infty[1-\mathrm{erf}(\varepsilon r\theta)]^2\mathrm{d}\theta=(4-2\sqrt{2})\pi^{3/2}\varepsilon^{-1}\quad \text{as } \varepsilon r\to\infty,\quad \varepsilon^2 r\to 0, \tag{5.44}$$

which is equal to the far-field value (5.43) as required by the conservation law (5.41*a*), despite the radically different scattering pattern. Most of the emitted energy is related to

the distortion component (5.30), as its transverse range is much greater than that of the radiation component. Thus, the scattered field identified with the radiation component by (2.30) violates (5.41*a*)

$$\sigma' \to 2\pi^2 r \int_0^{\infty} \left[1 - \operatorname{erf}\left(\frac{\mathrm{e}^{-\mathrm{i}\pi/4}\sqrt{r}\theta}{\sqrt{2}}\right)\right]^2 \mathrm{d}\theta \propto \sqrt{r} \quad \text{as } \varepsilon r \to \infty, \quad \varepsilon^2 r \to 0. \tag{5.45}$$

This is why, in this paper, we adhere to the terminology (2.13), (2.24) regarding the distortion component as a part of the scattered field despite its non-contribution to the interference pattern.

In the irrotational flow region, with (5.23) + (5.31) we have

$$\sigma \sim r \int_{-\pi}^{\pi} |\rho_{11}|^2 \cos\theta \,\mathrm{d}\theta \to 2\pi^2 r \int_0^{\infty} (1 - \theta/\pi)^2 \cos\theta \,\mathrm{d}\theta = 4\pi r \quad \text{as } \varepsilon r \to 0. \tag{5.46}$$

The momentum-transfer cross-section in the far field is equal to that in the near field and comparable to the wavelength so that

$$\sigma_{\infty}^{*} \to \pi^2/2, \tag{5.47}$$

as the distortion component and small angles do not contribute (Fabrikant 1982). Owing to this, Pitaevskii (1959) and Fetter (1964) obtained the correct value (5.47) based on the incorrect expression (i) for case PWPV. The result (5.47) was used to calculate the mutual friction force in superfluid helium.

5.4. *For the case* $\Gamma = 1$

In § 5.3 we have shown that expressions (i) and (ii) appearing in case PWPV $\Gamma = 1$ are included in the leading-order solution for the case $\Gamma = \exp(-\varepsilon^2 r^2)$ as $\varepsilon \to 0$ in the different regions (table 2). Now we explain what happens when one assumes $\varepsilon = 0$ and deals with the ill-posed RP using methods correct only for $\varepsilon > 0$ (as has been done in works devoted to the case PWPV).

In the degenerate case $\varepsilon = 0$, the only characteristic spatial scale for the source and hence for the scattered field is the acoustic wavelength $O(1)$. The source Fourier transform (5.10) for $\Gamma = 1$ is singular at the incident wave vector $\hat{\boldsymbol{k}}$

$$\widehat{q}_{11}(\boldsymbol{K}) = -2\mathrm{i}\frac{\boldsymbol{K}\cdot\hat{\boldsymbol{k}}\,\hat{\boldsymbol{z}}\cdot(\boldsymbol{K}\times\hat{\boldsymbol{k}})}{|\boldsymbol{K}-\hat{\boldsymbol{k}}|^2}. \tag{5.48}$$

(Generally, the source Fourier transform (5.10) and, hence, the scattering amplitude (5.8) is regular on the incident direction $\hat{\boldsymbol{r}} = \hat{\boldsymbol{k}}$ under the condition $|\boldsymbol{v}_{10}| = O(r^{-n})$, $n > 2$ as $r/R \to \infty$, which is the more rigorous than (3.10) for the well-posedness of the RP in the case of a uniform plane incident wave (4.8*a–c*). This suggests that in the case of the vortex velocity field $|\boldsymbol{v}_{10}| \propto r^{-n}$ for $3/2 < n \leq 2$ the usage of asymptotics (3.7) for Green's function is still not permitted, meaning that all the fluid must be considered as the flow region.)

The substitution of (5.48) into the far-field representation (5.7), (5.8) leads to expression (i), which is defined by (5.15)

$$f = f^{(i)}, \tag{5.49}$$

being singular on the line that represents the degenerated region $\theta/\varepsilon = O(1)$, so that

$$f^{(i)} \to \infty \quad \text{as } \theta \to 0. \tag{5.50}$$

As Berthet & Lund (1995) noted, the singularity is the indeterminate form $\infty - \infty$ (see figure 4). Expression (i) satisfies the radiation condition (3.4) but violates the Helmholtz equation (3.1), which is essentially inhomogeneous. In fact, the far-field representation breaks down because the asymptotics (3.7) for Green's function cannot be used in the flow region (Sakov 1993), the contribution of the sources within the neighbourhood $|\boldsymbol{r} - \boldsymbol{r}'| = O(1)$ is not correctly taken into account, and the property of Green's function to be the fundamental solution to the equation is lost.

The substitution of (5.48) into the exact representation (5.4) with (5.5) leads to expression (ii) defined by (5.23) + (5.31), which is non-decaying within the infinite region that represents the region of geometrical acoustics extended unboundedly, i.e.

$$|\boldsymbol{U}_{11}| = O(1) \quad \text{as } r \to \infty. \tag{5.51}$$

In the leading-order approximation, expression (ii) satisfies the inhomogeneous Helmholtz equation (3.1) but violates the radiation condition (3.4), even if one includes only the radiation component (5.23) into the scattered field. In fact, the exact representation (5.4) breaks down because expression (ii) violates the decay condition (3.5) and hence the equation (5.2). Other researchers using expression (ii) used different representations that also violated the radiation condition (3.4).

To summarise, neither the far-field representation (5.7), (5.8) nor the exact representation (5.4) is valid for case PWPV and neither expression (i) nor (ii) satisfies (3.1) and (3.4). Nevertheless, expression (ii) has the advantage that it corresponds to the region of geometrical acoustics including the region $\varepsilon r \to 0$ where $\Gamma \to 1$, as for case PWPV. In contrast, expression (i) corresponds to the far field where $\Gamma \to 0$, which is absent in case PWPV.

6. Conclusions

This work arose from the issue with the well-known problem of a uniform plane acoustic wave scattering by a point vortex, which was recognised as ill-posed because of the slowly decaying velocity field. In the framework of the Born approximation we showed that a two-dimensional scattering problem with the Sommerfeld radiation condition is well-posed if and only if the incident wave velocity field multiplied by the vortex velocity field is $o(r^{-3/2})$ as $r \to \infty$. This is fulfilled for any realisable statement but not for the case described previously. There is no contradiction: in unbounded space the kinetic energy of a two-dimensional flow with non-zero total circulation as well as the energy flux of the uniform plane wave is infinite so that neither of them can exist. This situation is specific for the two-dimensional case, without a clear analogue in three dimensions (see Smith & Ford 2001).

To obtain to a well-posed problem, we effectively constrict the flow induced by a point vortex to the region $r/L = O(1)$, where L was assumed long compared with the acoustic wavelength λ. More precisely, we utilised the vortex that emerged when an elongated solid circular cylinder of small radius compared with wavelength, rotated in a viscous fluid for a long time. The velocity field of such vortex is proportional to $r^{-1}\exp(-r^2/L^2)$. This is similar to a point vortex within the region $r \ll L$, where $L \propto \sqrt{t}$ can be made arbitrarily

large by increasing the rotation time t. The exponential decay as $r/L \to \infty$ ensures the well-posedness of the scattering problem.

For the case described, we obtained a leading-order solution as $\lambda/L \to 0$ by evaluation of exact integral representations and validated it by numerical integration. The solution has no singularities, satisfies the radiation condition and possesses finite energy flux. In addition, in different asymptotic regions it is reduced to expression (i) with a singularity on $\theta = 0$, and to expression (ii) which does not decay as $r \to \infty$, both are known from existing works on the case of a point vortex that nominally corresponds to $L = \infty$.

The overall scattering pattern (figures 2 and 6) is similar to the pattern of a plane wave diffraction by a slit of width L. In the far field (the Fraunhofer region) $r \gg L^2/\lambda$, the acoustic field is a uniform plane incident wave plus an outgoing cylindrical scattered wave. The scattering amplitude (5.14), (5.15) peaks at small scattering angles $\theta = O(\lambda/L)$, where it increases by $O(L/\lambda)$ (figures 4 and 7). At large angles $\theta \gg \lambda/L$, it matches expression (i). In the region of geometrical acoustics $r \ll L^2/\lambda$, the acoustic field is a non-uniform plane wave (5.26)–(5.28) (figure 5) plus the wave (5.23) which is non-decaying within the narrow parabolic region $\theta = O(\sqrt{\lambda/r})$, and outgoing cylindrical beyond. The energy flux conservation in the region $r \gg L$ unambiguously defines the component that provides the refraction of the incident wave as the part of the scattered field. In the subregion $|x| \ll L^2/\lambda$, $|y| \ll L$ that includes $r \ll L$ where the vortex velocity field is proportional to r^{-1}, the scattered field matches expression (ii). The presence of the spatial scale L^2/λ, long compared with the largest spatial scale L present in the problem statement, specifies the size of the domain that would have to be resolved in an experimental or numerical study.

To summarise, in the region $r \ll L$ where the flow is similar to that is induced by a point vortex the solution is reduced to expression (ii). In the region $r \gg L$ where the fluid is at rest the scattering pattern is quite complex (figure 6) and includes the region with expression (i) as well as the region with expression (ii) (table 2). Thus, the region corresponding to expression (i) is completely absent, whereas the part of the region corresponding to expression (ii) takes up all the space in the case of a point vortex. This suggests we regard expression (ii) as in some sense relevant, whereas expression (i) is regarded as irrelevant to the case of to point vortex.

The formulation considered in this paper is analogous to that with a vortex velocity field proportional to $r^{-1}\exp(-r/L)$ proposed by Berthet & Lund (1995) and in addition has a clear physics-based rationale. Berthet & Lund (1995) succeeded in obtaining the far-field solution (5.16), (5.15), analogous to (5.14), (5.15). Following the strategy of the present paper, one could obtain the corresponding solution in the region of geometrical acoustics, which is expected to be analogous to (5.23) + (5.26) but perhaps would need more cumbersome calculations.

Acknowledgements. We thank the three anonymous reviewers for their valuable comments on our manuscript.

Funding. The reported study was funded by RFBR, project number 19-31-90057.

Declaration of interests. The authors report no conflict of interest.

Author ORCIDs.
Dmitry A. Gadzhiev https://orcid.org/0000-0002-3398-8612.

Appendix A. Derivation of the solution for the case $\Gamma = \exp(-\varepsilon^2 r^2)$

The leading-order solution to the RP with the source (4.11) for $\Gamma = \exp(-\varepsilon^2 r^2)$ as $\varepsilon \to 0$ is derived using the exact representation (5.4) with the bypass rule (5.5) for the source Fourier transform (5.13). We follow the method developed by Ford & Smith (1999) and Howe (1999) for case PWPV corresponding to $\varepsilon = 0$.

A.1. *Exact representation through a single integral*

The solution (5.4), (5.13) is represented as the sum of two terms

$$\rho_{11} = \rho_{11}^{p} + \rho_{11}^{c}, \tag{A1}$$

$$\rho_{11}^{p} = -\frac{\mathrm{i}}{2\pi}\int_{\mathbb{R}^2} \frac{\boldsymbol{K}\cdot\hat{\boldsymbol{k}}\,\hat{\boldsymbol{z}}\cdot(\boldsymbol{K}\times\hat{\boldsymbol{k}})}{1-\boldsymbol{K}\cdot\hat{\boldsymbol{k}}} \frac{(1-\exp(-|\boldsymbol{K}-\hat{\boldsymbol{k}}|^2/4\varepsilon^2))}{|\boldsymbol{K}-\hat{\boldsymbol{k}}|^2}\exp(\mathrm{i}\boldsymbol{K}\cdot\boldsymbol{r})\,\mathrm{d}^2\boldsymbol{K}, \tag{A2}$$

$$\rho_{11}^{c} = -\frac{\mathrm{i}}{2\pi}\int_{\mathcal{C}} \frac{\boldsymbol{K}\cdot\hat{\boldsymbol{k}}\,\hat{\boldsymbol{z}}\cdot(\boldsymbol{K}\times\hat{\boldsymbol{k}})}{1-\boldsymbol{K}\cdot\hat{\boldsymbol{k}}} \frac{(1-\exp(-|\boldsymbol{K}-\hat{\boldsymbol{k}}|^2/4\varepsilon^2))}{1-K^2}\exp(\mathrm{i}\boldsymbol{K}\cdot\boldsymbol{r})\,\mathrm{d}^2\boldsymbol{K}, \tag{A3}$$

with the pole $\kappa = 1$ bypassed with the rule $\mathrm{Im}(\kappa) < 0$, consistent with (5.5).

The integral (A2) is the inverse Fourier transform of the function $\widehat{q}_{11}(\kappa,\mu)/2(1-\kappa)$. Under the bypass rule used, the transform of $1/2(1-\kappa)$ is equal to $-\pi\mathrm{i}\,\mathrm{e}^{\mathrm{i}x}\mathcal{H}(x)\delta(y)$, where $\mathcal{H}(x)$ is the Heaviside step function and $\delta(y)$ is the Dirac delta function. Applying the convolution theorem and substituting (4.11) and (4.12) for $q_{11}(x,y)$, we obtain exactly

$$\begin{aligned}\rho_{11}^{p} &= -\exp(\mathrm{i}\hat{\boldsymbol{k}}\cdot\boldsymbol{r})\left\{\mathrm{i}\int_{-\hat{\boldsymbol{k}}\infty}^{\boldsymbol{r}} \hat{\boldsymbol{k}}\cdot\boldsymbol{v}_{10}(\boldsymbol{r}')\hat{\boldsymbol{k}}\cdot\mathrm{d}\boldsymbol{r}' + \hat{\boldsymbol{k}}\cdot\boldsymbol{v}_{10}(\boldsymbol{r})\right\}\\ &= \mathrm{e}^{\mathrm{i}x}\left\{\pi\mathrm{i}\left[2T(\sqrt{2}\varepsilon y, x/y) + \frac{1}{2}\left(\mathrm{sgn}(y) - \mathrm{erf}(\varepsilon y)\right)\right] + \frac{y}{x^2+y^2}\exp(-\varepsilon^2(x^2+y^2))\right\},\end{aligned} \tag{A4}$$

where

$$T(\zeta, a) = \frac{1}{2\pi}\int_0^a \frac{\exp(-\zeta^2(1+x'^2)/2)}{1+x'^2}\mathrm{d}x' \tag{A5}$$

is the Owen T-function (Owen 1956, for its properties see Brychkov & Savischenko 2016). The singularity in (A4) is owing to the point vortex.

In the expression (A3), we integrate with respect to μ passing the poles $\mu = \pm\sqrt{1-\kappa^2}$ and choose the analytic branch of the function $\sqrt{\kappa^2-1}$, consistent with (5.5). The solution is represented as the Sommerfeld integral in terms of the variable $\psi = \xi + \mathrm{i}\eta$ defined by $\kappa = \cos\psi$, $\mathrm{i}\sqrt{\kappa^2-1} = \sin\psi$ so that

$$\rho_{11}^{c} = \rho_{11}^{c,0} + \rho_{11}^{c,1}, \tag{A6}$$

$$\begin{aligned}\rho_{11}^{c,0} &= \frac{\mathrm{i}}{2\pi}\mathrm{sgn}(y)\int_{-\infty}^{\infty}\frac{\kappa}{1-\kappa}\mathrm{e}^{\mathrm{i}\kappa x}\left(\int_{-\infty}^{\infty}\frac{\mu}{1-\kappa^2-\mu^2}\mathrm{e}^{\mathrm{i}\mu|y|}\,\mathrm{d}\mu\right)\mathrm{d}\kappa\\ &= \frac{\mathrm{sgn}(y)}{2}\int_{-\infty}^{\infty}\frac{\kappa}{1-\kappa}\exp(-\sqrt{\kappa^2-1}|y| + \mathrm{i}\kappa x)\,\mathrm{d}\kappa\\ &= -\frac{\mathrm{sgn}(\theta)}{2}\int_{C}\exp(\mathrm{i}r\cos(\psi-|\theta|))\cos\psi\cot\frac{\psi}{2}\,\mathrm{d}\psi,\end{aligned} \tag{A7}$$

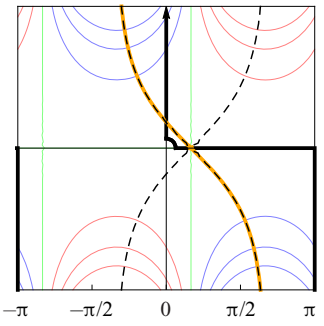

Figure 11. The integration contours for (A7) in the complex plane ψ for $\theta = \pi/6$: the original contour C (black, thick) and the SDP C_0 (orange). Thin coloured curves are $\mathrm{Re}(E_0(\psi)) = 0, \pm 0.5, \pm 1, \pm 1.5$; blue curves correspond to negative values, green to zero and red to positive values. Dashed curves are $\mathrm{Im}(E_0(\psi)) = \mathrm{Im}(E_0(\psi_{s,0}))$.

$$\begin{aligned}
\rho_{11}^{c,1} &= -\frac{\mathrm{i}}{2\pi}\mathrm{sgn}(y)\int_{-\infty}^{\infty}\frac{\kappa}{1-\kappa}\exp(-(\kappa-1)^2/4\varepsilon^2) \\
&\quad\times \mathrm{e}^{\mathrm{i}\kappa x}\left(\int_{-\infty}^{\infty}\frac{\mu}{1-\kappa^2-\mu^2}\mathrm{e}^{-\mu^2/4\varepsilon^2}\,\mathrm{e}^{\mathrm{i}\mu|y|}\,\mathrm{d}\mu\right)\mathrm{d}\kappa \\
&= \rho_{11}^{c,1|+} + \rho_{11}^{c,1|-}, \\
\rho_{11}^{c,1|\pm} &= \frac{\mathrm{sgn}(y)}{2}\int_{-\infty}^{\infty}F_{\pm}\frac{\kappa}{1-\kappa}\exp(\mp\sqrt{\kappa^2-1}|y| + \mathrm{i}\kappa x)\,\mathrm{d}\kappa \\
&= -\frac{\mathrm{sgn}(\theta)}{2}\int_C F_{\pm}\exp(\mathrm{i}r\cos(\psi\mp|\theta|))\cos\psi\cot\frac{\psi}{2}\,\mathrm{d}\psi, \qquad \text{(A8)} \\
F_{\pm} &= \mp\frac{1}{2}\exp((\kappa-1)/2\varepsilon^2)\left[1+\mathrm{erf}\left(-\frac{\sqrt{\kappa^2-1}}{2\varepsilon}\pm\varepsilon|y|\right)\right] \\
&= \mp\frac{1}{2}\exp(-\sin^2(\psi/2)/\varepsilon^2)\left[1+\mathrm{erf}\left(\frac{\mathrm{i}\sin\psi}{2\varepsilon}\pm\varepsilon r\sin|\theta|\right)\right]. \qquad \text{(A9)}
\end{aligned}$$

The integration contour C in (A7), (A8) consists of three straight lines

$$\psi = \pi + \mathrm{i}\eta, \quad -\infty < \eta \le 0; \quad \psi = \xi, \quad \pi \ge \xi > 0; \quad \psi = \mathrm{i}\eta, \quad 0 < \eta < \infty \qquad \text{(A10}a\text{–}c\text{)}$$

and an infinitely small arc passing the pole $\psi = 0$ counter-clockwise (figures 11–12).

The exact representation (A1) and (A4)–(A10) is used to calculate the numerical solution, especially in the near field where the analytical expression is unknown. The important region for the integration is $\mathrm{Im}(\psi) = O(1)$ for (A7) and $\psi = O(\sqrt{\varepsilon})$ for (A8). The contribution of the arc is equal to the residue of the integrand at $\psi = 0$ multiplied by $\pi\mathrm{i}/2$.

A.2. *Leading-order solution as $\varepsilon \to 0$, $r \to \infty$*

The expression (A4) as $r \to \infty$ is reduced to (5.26) that constitutes the distortion component in the region of geometrical acoustics $\varepsilon^2 r \to 0$.

To calculate (A7) and (A8) as $r \to \infty$, we use the stationary-phase method (Borovikov 1994): The contour C is deformed on to the steepest descent path (SDP) C_* specified by

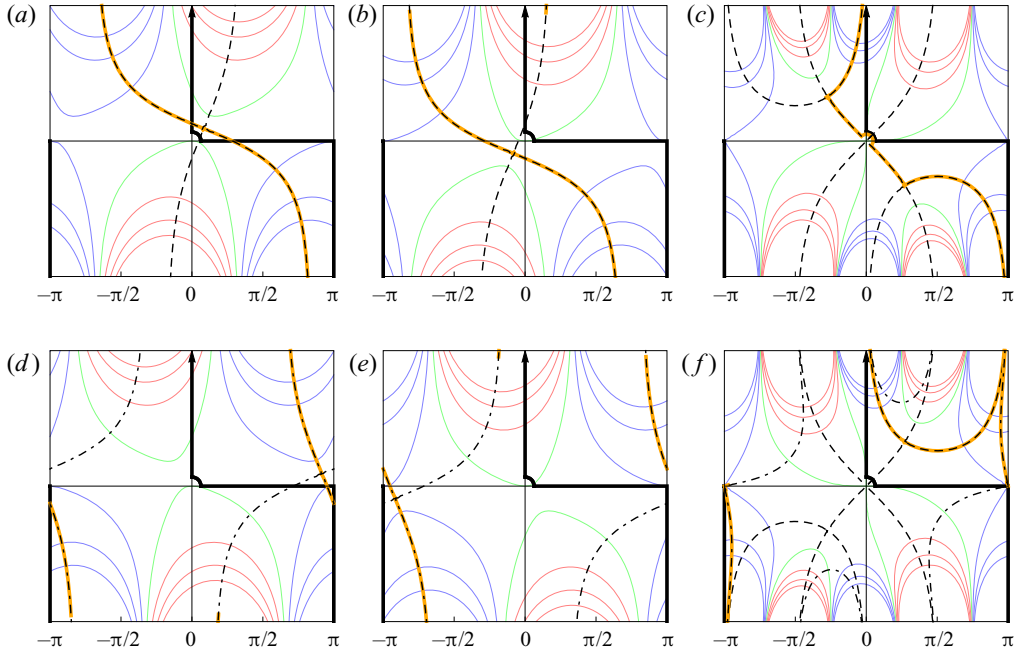

Figure 12. The integration contours for (A8) in the complex plane ψ for $r = 0.5$ and $\theta = \pi/6$ (*a–c*), $\theta = 5\pi/6$ (*d–f*): the original contour C (black, thick) and the auxiliary SDPs $C^n_{1|+}$ (*a*, *d*), $C^n_{1|-}$ (*b*,*e*), C^f_1 (*c*,*f*) (orange). Thin coloured curves are $\mathrm{Re}(E_*(\psi)) = n\varepsilon^{-2}$, $n = 0, \pm1, \pm2, \pm3$; blue curves correspond to negative values, green to zero, and red for positive values (A16*a*,*b*). Dashed and dash-dotted curves are $\mathrm{Im}(E_*(\psi)) = \mathrm{Im}(E_*(\psi^n_{s,*}))$ corresponding to the different $\mathrm{Im}(E_*(\psi^n_{s,*}))$.

the most highly oscillatory factor $\exp(E_*(\psi))$ in the integrand of the term $\rho^{c,*}_{11}$. SDP is defined as the contour that passes through the saddle point $\psi_{s,*}$, such that

$$\mathrm{d}E_*/\mathrm{d}\psi = 0 \quad \text{for } \psi = \psi_{s,*}, \tag{A11}$$

in the direction in which

$$\mathrm{Im}(E_*(\psi)) = \mathrm{Im}(E_*(\psi_{s,*})), \quad \mathrm{Re}(E_*(\psi)) \le \mathrm{Re}(E_*(\psi_{s,*})) \quad \text{for } \psi \in C_*. \tag{A12a,b}$$

In figures 11 and 12 saddle points are intersections of curves $\mathrm{Im}(E_*(\psi)) = \mathrm{Im}(E_*(\psi_{s,*}))$. As $r \to \infty$, a high increment in $E_*(\psi)$ for (A7) and (A8) ensures that only a neighbourhood of the saddle point $|\psi - \psi_{s,*}| \to 0$ contributes to the integral along C_*.

In the case of the continuous deformation, the integral along C is equal to that along C_*. In the case when the contour crosses the pole $\psi = 0$, the integral changes by the respective residue of the integrand multiplied by $2\pi\mathrm{i}$. The deformation with crossing the infinite-range zones where the integrand is growing unlimitedly is not permitted. As the integrands are 2π-periodic, the complex space ψ is an isomorphism of a cylinder rather than of a plane, so we distinguish between deformations in clockwise and counter-clockwise directions.

A.2.1. *Calculation of* (A7)

For the term $\rho^{c,0}_{11}$, the most highly oscillatory factor and the saddle points defined by (A11) are

$$E_0(\psi) = \mathrm{i}r\cos(\psi - |\theta|); \quad \psi_{s,0} = |\theta|, \quad \psi'_{s,0} = |\theta| - \pi. \tag{A13a–c}$$

The SDP that can be obtained by a continuous deformation of C passes through $\psi_{s,0}$ and is determined from (A12) by

$$\psi = |\theta| + \tau + \mathrm{i}\ln\frac{1-\sin\tau}{\cos\tau} \quad \text{on } C_0, \quad -\pi/2 < \tau < \pi/2, \tag{A14}$$

as shown in figure 11. Substituting (A14) into (A7) and using approximations $\psi \to |\theta| + \sqrt{2}\mathrm{e}^{-\mathrm{i}\pi/4}\tau$ as $\tau \to 0$ and so on, we obtain

$$\begin{aligned}\rho_{11}^{c,0} &\sim \frac{\mathrm{sgn}(\theta)}{\sqrt{2}}\exp(\mathrm{i}r - \mathrm{i}\pi/4)\cos\theta\int_{-\infty}^{\infty}\mathrm{e}^{-r\tau^2}\cot\frac{|\theta| + \sqrt{2}\mathrm{e}^{-\mathrm{i}\pi/4}\tau}{2}\,\mathrm{d}\tau \\ &\sim \begin{cases} -\pi\mathrm{i}\exp(\mathrm{i}r(1-\theta^2/2))\left[\mathrm{sgn}(\theta) - \mathrm{erf}\left(\dfrac{\mathrm{e}^{-\mathrm{i}\pi/4}\sqrt{r}\theta}{\sqrt{2}}\right)\right] & \text{as } \sqrt{r}\theta = O(1), \\ \sqrt{\dfrac{\pi}{2r}}\exp(\mathrm{i}r - \mathrm{i}\pi/4)\cos\theta\cot\dfrac{\theta}{2} & \text{as } \theta = O(1). \end{cases}\end{aligned} \tag{A15}$$

The multiplicative composition of the matched expansions in (A15), meaning their multiplication divided by the intermediate approximation (see Van Dyke (1964), § 5.10), yields the uniformly valid solution (5.23) that constitutes the radiation component in the region of geometrical acoustics $\varepsilon^2 r \to 0$.

Thus $\rho_{11}^{p} + \rho_{11}^{c,0}$ is the solution (5.23) + (5.26) in the region of geometrical acoustics $\varepsilon^2 r \to 0$.

A.2.2. *Calculation of* (A8)

For the terms $\rho_{11}^{c,1|\pm}$, the most highly oscillatory factor is difficult to define explicitly because of the error function in (A9). For understanding the behaviour of the SDP, let us consider two simplified cases when the error function is replaced with its approximation in the near or far region, using the indices 'n' and 'f', respectively.

In case n, the factor with the error function in (A9) is assumed constant. The most highly oscillatory factor and the saddle points defined by (A11) are

$$E_{1|\pm}^{n}(\psi) = \mathrm{i}r\cos(\psi \mp |\theta|) - \sin^2(\psi/2)/\varepsilon^2; \quad \psi_{s,1|\pm}^{n} = -\frac{\mathrm{i}}{2}\ln\frac{2\mathrm{i}\varepsilon^2 r\mathrm{e}^{\pm\mathrm{i}|\theta|} + 1}{2\mathrm{i}\varepsilon^2 r\mathrm{e}^{\mp\mathrm{i}|\theta|} + 1}, \tag{A16a,b}$$

where $\psi_{s,1|+}^{n}$ as well as $\psi_{s,1|-}^{n}$ include two saddle points separated by π, corresponding to two different branches of the complex logarithm. At each of them,

$$E_{1|\pm}^{n}(\psi_{s,1|\pm}^{n}) = -(1 - \sqrt{1 + 4\mathrm{i}\varepsilon^2 r\cos\theta - 4(\varepsilon^2 r)^2})/2\varepsilon^2 \tag{A17}$$

and the inclination angle to x-axis is $-(1/4)\mathrm{arccot}[(1 - 4(\varepsilon^2 r)^2)/(4\varepsilon^2 r\cos\theta)]$. The SDP that can be obtained by a permissible deformation of C passes through the saddle point whose real part lies within 0 and $\pm\pi$. Typical SDPs $C_{1|+}^{n}$ and $C_{1|-}^{n}$, antisymmetric to each other with respect to origin, are shown in figure 12(a,b,d,e). $C_{1|+}^{n}$ approaches C_0 as $\varepsilon^2 r \to \infty$ and the piecewise rectilinear contour $\psi = \pi + \mathrm{i}\eta,\ -\infty < \eta \le 0;\ \psi = \xi,\ \pi \ge \xi \ge -\pi;\ \psi = -\pi + \mathrm{i}\eta,\ 0 < \eta < \infty$ as $\varepsilon^2 r \to 0$.

In case f, the factor with the error function in (A9) is replaced with its asymptotics

$$1+\mathrm{erf}(\phi)\to-\exp(-\phi^2)/(\sqrt{\pi}\phi)\quad\text{as }\phi\to\infty\quad\text{unless}\quad-\pi/4\le\arg(\phi)\le\pi/4, \tag{A18}$$

which is achieved along the contour C. The most highly oscillatory factor and the saddle points defined by (A11) are equal for $\rho_{11}^{c,1|+}$ and $\rho_{11}^{c,1|-}$

$$\left.\begin{aligned} E_1^f(\psi)&=-\varepsilon^2r^2\sin^2\theta+\mathrm{i}r\cos\theta\cos\psi-\sin^4(\psi/2)/\varepsilon^2;\\ \psi_{s,1}^f&=0,\quad \psi_{s,1}^{f'}=\pi,\quad \psi_{s,1}^{f\pm}=\pm\arccos(1+2\mathrm{i}\varepsilon^2r\cos\theta).\end{aligned}\right\} \tag{A19}$$

Owing to the quartic term, the SDP is a piecewise smooth curve qualitatively different for $|\theta|<\pi/2$ and $|\theta|>\pi/2$.

For $|\theta|<\pi/2$, C_1^f passes through the points $\psi_{s,1}^f$ (turning around it counter-clockwise), $\psi_{s,1}^{f+}$ and $\psi_{s,1}^{f-}$ (figure 12*c*). The part between $\psi_{s,1}^{f+}$ and $\psi_{s,1}^{f-}$ is given by (A14) for $\theta=0$. Reaching $\psi_{s,1}^{f+}$ and $\psi_{s,1}^{f-}$ with the inclination angle $-(1/2)\mathrm{arccot}(-\varepsilon^2r\cos\theta)$ to x-axis, C_1^f turns by 90° to stay within the region where the integrand is decaying. At infinity, it approaches C. The peak value of the integrand is reached at the point $\psi_{s,1}^f$

$$\mathrm{Re}(E_1^f(\psi_{s,1}^f))=-\varepsilon^2r^2\sin^2\theta,\quad \mathrm{Re}(E_1^f(\psi_{s,1}^{f\pm}))=-\varepsilon^2r^2. \tag{A20a,b}$$

The contour C_1^f approaches C as $\varepsilon^2r\to0$ and unboundedly extends its C_0-like part as $\varepsilon^2r\to\infty$.

For $|\theta|>\pi/2$, C_1^f consists of two parts with different values of $\mathrm{Im}(E_1^f(\psi))$ (figure 12*f*) attached to each other at a point close to $\pi+\mathrm{i}\eta$, $\eta\gg1$, where the integrand is negligible. The part with $\mathrm{Im}(E_1^f(\psi))=-r\cos\theta$ passes through the saddle point $\psi_{s,1}^{f'}$, whereas the part with $\mathrm{Im}(E_1^f(\psi))=r\cos\theta$ through the point $\psi_{s,1}^{f+}$. The peak value of the integrand is reached at $\psi_{s,1}^{f+}$ and defined by (A20*b*).

The real SDP $C_{1|\pm}$ is believed to be similar to $C_{1|\pm}^n$ near the saddle point defined by (A16*b*) and to C_1^f far from it. The integral along $C_{1|\pm}$ is equal to that along $C_{1|\pm}^n$, as only the neighbourhood of the saddle point contributes. The behaviour of C_1^f specifies the direction of the contour deformation, clockwise or counter-clockwise, that avoids crossing the infinite-range zones where the integrand is growing unlimitedly. Comparison of figures 12(*a*,*b*) against 12(*c*) and of 12(*d*,*e*) against 12(*f*) shows that C is deformed on to $C_{1|+}$ continuously either for $|\theta|<\pi/2$ and for $|\theta|>\pi/2$, while on to $C_{1|-}$ crossing the pole $\psi=0$ for $|\theta|<\pi/2$ and continuously for $|\theta|>\pi/2$.

Now let us consider calculation of $\rho_{11}^{c,1}$. First, (A8)–(A9) indicates that

$$\rho_{11}^{c,1|-}\sim-\rho_{11}^{c,1|+}\quad\text{as }\varepsilon y\to0. \tag{A21}$$

In addition, at the analytic branch of (A17) corresponding to the previously used SDP,

$$\mathrm{Re}(E_{1|\pm}^n(\psi_{s,1|\pm}^n))\to-\infty\quad\text{as}\quad\begin{cases}\theta/\varepsilon\to\infty, & \varepsilon^2r=O(1)\quad\text{or }\varepsilon^2r\to\infty,\\ \sqrt{r}\theta\to\infty, & \varepsilon^2r\to0.\end{cases} \tag{A22}$$

Under the condition (A22), the terms $\rho_{11}^{c,1|\pm}$ are exponentially decaying. To summarise (A21) and (A22), we have

$$\rho_{11}^{c,1}\to0\quad\text{as }\varepsilon^2r\to0\quad\text{or}\quad\theta/\varepsilon\to\infty. \tag{A23}$$

This proves that the solution (5.23) + (5.26) is valid in the region of geometrical acoustics as well as at large angles in the near field, where it is reduced to (5.36).

In the far field $\varepsilon^2 r \to \infty$, the important part of the SDP $C_{1|+}$ approaches C_0, whereas the important part of $C_{1|-}$ the contour antisymmetric to C_0 with respect to origin. We follow the derivation of (A15) by taking (A9) at the saddle point $\psi = \pm|\theta|$. To $\rho_{11}^{c,1|-}$, for $|\theta| < \pi/2$ we add the residue of the integrand at the pole $\psi = 0$ multiplied by $2\pi\mathrm{i}$, thus

$$\rho_{11}^{c,1|+} \sim -\tfrac{1}{2}\exp(-\theta^2/4\varepsilon^2)\,[1 + \operatorname{erf}(\varepsilon r \sin|\theta|)]\,\rho_{11}^{c,0}, \tag{A24a}$$

$$\begin{aligned}\rho_{11}^{c,1|-} \sim\ & -\pi\mathrm{i}\exp(\mathrm{i}r\cos\theta)\mathcal{H}(\cos\theta)\left[\operatorname{sgn}(\theta) - \operatorname{erf}(\varepsilon r\sin\theta)\right] \\ & -\tfrac{1}{2}\exp(-\theta^2/4\varepsilon^2)\,[1 - \operatorname{erf}(\varepsilon r\sin|\theta|)]\,\rho_{11}^{c,0} \quad \text{as } \varepsilon^2 r \to \infty.\end{aligned} \tag{A24b}$$

The sum of (A24*a*) and (A24*b*) is

$$\begin{aligned}\rho_{11}^{c,1} \sim\ & -\pi\mathrm{i}\exp(\mathrm{i}r\cos\theta)\mathcal{H}(\cos\theta)[\operatorname{sgn}(\theta) - \operatorname{erf}(\varepsilon r\sin\theta)] \\ & -\exp(-\theta^2/4\varepsilon^2)\rho_{11}^{c,0} \quad \text{as } \varepsilon^2 r \to \infty.\end{aligned} \tag{A25}$$

The first term in (A25) cancels out (5.26), while the sum of the second and (5.23) in the leading-order approximation is equivalent to the far-field solution (5.7), (5.14), (5.15).

References

Aharonov, Y. & Bohm, D. 1959 Significance of electromagnetic potentials in the quantum theory. *Phys. Rev.* **115**, 485–491.

Balmforth, N.J., Smith, S.G.L. & Young, W.R. 1998 Enhanced dispersion of near-inertial waves in an idealized geostrophic flow. *J. Mar. Res.* **56**, 1–40.

Belyaev, I.V. & Kopiev, V.F. 2008 On the statement of the problem of sound scattering by a cylindrical vortex. *Acoust. Phys.* **54**, 603–614.

Berry, M.V., Chambers, R.G., Large, M.D., Upstill, C. & Walmsley, J.C. 1980 Wavefront dislocations in the Aharonov-Bohm effect and its water wave analogue. *Eur. J. Phys.* **1**, 154–162.

Berthet, R. & Coste, C. 2003 Using a partial-wave method for sound–mean-flow scattering problems. *Phys. Rev.* E **67**, 036604.

Berthet, R., Fauve, S. & Labbé, R. 2003 Study of the sound-vortex interaction: direct numerical simulations and experimental results. *Eur. Phys. J.* B **32**, 237–242.

Berthet, R. & Lund, F. 1995 The forward scattering of sound by vorticity. *Phys. Fluids* **7**, 2522–2524.

Blokhintsev, D.I. 1946 Acoustics of a nonhomogeneous moving medium. *NACA Tech. Memo.* 1399.

Borovikov, V.A. 1994 *Uniform Stationary Phase Method*. Institution of Electrical Engineers.

Brychkov, Y.A. & Savischenko, N.V. 2016 Some properties of the owen t-function. *Integr. Transf. Spec. F.* **27**, 163–180.

Bühler, O. & McIntyre, M.E. 2003 Remote recoil: a new wave-mean interaction effect. *J. Fluid Mech.* **492**, 207–230.

Candel, S.M. 1979 Numerical solution of wave scattering problems in the parabolic approximation. *J. Fluid Mech.* **90**, 465–507.

Clair, V. & Gabard, G. 2015 Numerical assessment of the scattering of acoustic waves by turbulent structures. In *21st AIAA/CEAS Aeroacoustics Conference*, p. 2680. AIAA.

Colonius, T., Lele, S.K. & Moin, P. 1994 The scattering of sound waves by a vortex: numerical simulations and analytical solutions. *J. Fluid Mech.* **260**, 271–298.

Coste, C., Lund, F. & Umeki, M. 1999 Scattering of dislocated wave fronts by vertical vorticity and the Aharonov-Bohm effect. I. Shallow water. *Phys. Rev.* E **60**, 4908–4916.

Doronina, O.A. & Zhdanova, N.S. 2013 Numerical simulation of acoustic waves scattering by isolated vortex structures. *Math. Models Comput. Simul.* **25**, 85–94.

Fabrikant, A.L. 1982 Sound scattering by a vortex. *Sov. Phys. Acoust.* **28**, 694–695.

Fabrikant, A.L. 1983 Sound scattering by vortex flows. *Sov. Phys. Acoust.* **29**, 152–155.

Fedoryuk, M.V. 1963 The stationary phase method for multidimensional integrals. *Zh. Vych. Mat.* **2**, 145–150.

FERZIGER, J.H. 1974 Low-frequency acoustic scattering from a trailing vortex. *J. Acoust. Soc. Am.* **56**, 1705–1707.

FETTER, A.L. 1964 Scattering of sound by a classical vortex. *Phys. Rev.* **136**, 1488–1493.

FORD, R. 1994 Gravity wave radiation from vortex trains in rotating shallow water. *J. Fluid Mech.* **281**, 81–118.

FORD, R. & SMITH, S.G.L. 1999 Scattering of acoustic waves by a vortex. *J. Fluid Mech.* **386**, 305–328.

GADZHIEV, D.A., GAIFULLIN, A.M. & ZUBTSOV, A.V. 2020 On vortex generation by a rotating cylinder. *Fluid Dyn.* **55**, 965–981.

GAIFULLIN, A.M. 2015 *Vortex Flows* (in Russian). Nauka.

GOLEMSHTOK, G.M. & FABRICANT, A.L. 1980 Scattering and amplification of sound waves by cylindrical vortex. *Sov. Phys. Acoust.* **26**, 383–390.

GROMOV, P.R., EZERSKII, A.B. & FABRIKANT, A.L. 1982 Sound scattering by a vortex wake behind a cylinder. *Acoust. Phys.* **28**, 452–455.

HORNE, W. 1983 Measurements of the scattering of sound by a line vortex. *AIAA Paper* 1983-0676.

HOWE, M.S. 1975 Contributions to the theory of aerodynamic sound, with application to excess jet noise and the theory of the flute. *J. Fluid Mech.* **71**, 625–673.

HOWE, M.S. 1983 On the scattering of sound by a vortex ring. *J. Sound Vib.* **87**, 567–571.

HOWE, M.S. 1999 On the scattering of sound by a rectilinear vortex. *J. Sound Vib.* **227**, 1003–1017.

IWATSU, R. & TSURU, H. 2013 Numerical simulation of acoustic scattering from a circular vortex. *Theor. Appl. Mech. Japan* **61**, 95–104.

KAMBE, T. & OO, U.M. 1981 Scattering of sound by a vortex ring. *J. Phys. Soc. Japan* **50**, 3507–3516.

KARABASOV, S.A., KOPIEV, V.F. & GOLOVIZNIN, V.M. 2009 On a classical problem of acoustic wave scattering by a free vortex: numerical modelling. In *15th AIAA/CEAS Aeroacoustics Conference (30th AIAA Aeroacoustics Conference)*, p. 3234. AIAA.

KLIMOV, V.V. & PROZOROVSKII, V.L. 1987 Scattering of acoustic waves by a three-dimensional vortex. *Acoust. Phys.* **33**, 79–81.

KOP'EV, V.F. & CHERNYSHEV, S.A. 2000 Vortex ring oscillations, the development of turbulence in vortex rings and generation of sound. *Phys.-Usp.* **43**, 663–690.

KOPIEV, V.F. & BELYAEV, I.V. 2010 On long-wave sound scattering by a rankine vortex: non-resonant and resonant cases. *J. Sound Vib.* **329**, 1409–1421.

KOPIEV, V.F. & LEONTIEV, E.A. 1983 Acoustic instability of an axial vortex. *Sov. Phys. Acoust.* **29**, 192–198.

KOPIEV, V.F. & LEONTIEV, E.A. 1987 Radiation and scattering of sound from a vortex ring. *Fluid Dyn.* **22**, 83–95.

KRYLOV, V.V. 1989 *Basic Principles of Sound Radiation and Scattering* (in Russian). Moscow University Press.

LABBE, R. & PINTON, J.F. 1998 Propagation of sound through a turbulent vortex. *Phys. Rev. Lett.* **81**, 1413–1416.

LANDAU, L.D. & LIFSHITZ, E.M. 1987 *Fluid Mechanics*. Pergamon.

LIGHTHILL, M.J. 1953 On the energy scattered from the interaction of turbulence with sound or shock waves. *Math. Proc. Cambridge* **49**, 531–551.

LINDSAY, R.B. 1948 Compressional wave front propagation through a simple vortex. *J. Acoust. Soc. Am.* **20**, 89–94.

LUND, F. & ROJAS, C. 1989 Ultrasound as a probe of turbulence. *Physica* D **37**, 508–514.

MANNEVILLE, S., ROUX, P., TANTER, M., MAUREL, A., FINK, M., BOTTAUSCI, F. & PETITJEANS, P. 2001 Scattering of sound by a vorticity filament: an experimental and numerical investigation. *Phys. Rev.* E **63**, 036607.

MCINTYRE, M.E. 2009 Spontaneous imbalance and hybrid vortex–gravity structures. *J. Atmos. Sci.* **66**, 1315–1326.

MCINTYRE, M.E. 2019 Wave–vortex interactions, remote recoil, the Aharonov–Bohm effect and the Craik–Leibovich equation. *J. Fluid Mech.* **881**, 182–217.

MONIN, A.S. & YAGLOM, A.M. 2013 *Statistical Fluid Mechanics, Volume II: Mechanics of Turbulence*. Courier Corporation.

NAUGOLNYKH, K. 2013 Sound scattering by a vortex dipole. *J. Acoust. Soc. Am.* **133**, 1882–1884.

NAZARENKO, S.V. 1994 Absorption of sound by vortex filaments. *Phys. Rev. Lett.* **73**, 1793–1796.

NAZARENKO, S.V., ZABUSKY, N.J. & SCHEIDEGGER, T. 1995 Nonlinear sound–vortex interactions in an inviscid isentropic fluid: a two-fluid model. *Phys. Fluids* **7**, 2407–2419.

OSEEN, C.W. 1912 Uber die wirbelbewegung in einer reibenden flussigkeit. *Ark. Mat. Astron. Fys.* **7**.

O'SHEA, S. 1975 Sound scattering by a potential vortex. *J. Sound Vib.* **43**, 109–116.

OWEN, D.B. 1956 Tables for computing bivariate normal probabilities. *Ann. Math. Statist.* **27**, 1075–1090.

PITAEVSKII, L.P. 1959 Calculation of the phonon part of the mutual friction force in superfluid helium. *Sov. Phys. JETP* **8**, 888–890.

PLOUGONVEN, R. & ZEITLIN, V. 2002 Internal gravity wave emission from a pancake vortex: an example of wave–vortex interaction in strongly stratified flows. *Phys. Fluids* **14**, 1259–1268.

REINSCHKE, J., MÖHRING, W. & OBERMEIER, F. 1997 Scattering of sound waves by a cylindrical vortex: a semi-analytical theory. *J. Fluid Mech.* **333**, 273–299.

RELLICH, F. 1943 Über das asymptotische verhalten der lösungen von... $u + \ldots u = 0$ in unendlichen gebieten. *Jahresber. Dtsch. Math. Ver.* **53**, 57–65.

SAKOV, P.V. 1993 Sound scattering by a vortex filament. *Acoust. Phys.* **39**, 280–282.

SALANT, R.F. 1969 Acoustic rays in two-dimensional rotating flows. *J. Acoust. Soc. Am.* **46**, 1153–1157.

SCHOT, S.H. 1992 Eighty years of Sommerfeld's radiation condition. *Hist. Math.* **19**, 385–401.

SMITH, S.G.L. 1999 Near-inertial oscillations of a barotropic vortex: trapped modes and time evolution. *J. Phys. Oceanogr.* **29**, 747–761.

SMITH, S.G.L. 2002 Scattering of acoustic waves by a superfluid vortex. *J. Phys.* A **35**, 3597–3607.

SMITH, S.G.L. & FORD, R. 2001 Three-dimensional acoustic scattering by vortical flows. I. General theory. *Phys. Fluids* **13**, 2876–2889.

SOZOU, C. 1990 Resonant interaction of a sound wave with a cylindrical vortex. *J. Acoust. Soc. Am.* **87**, 2342–2348.

SVESHNIKOV, A.G., BOGOLYUBOV, A.N. & KRAVTSOV, V.V. 2004 *Lectures on Mathematical Physics* (in Russian). MSU.

TANAKA, K. & ISHII, S. 1982 Scattering of a plane sound wave by a vortex pair. *J. Phys. Soc. Japan* **51**, 1992–1999.

TATARSKI, V.I. 2016 *Wave Propagation in a Turbulent Medium*. Courier Dover Publications.

THOMAS, J. 2017 New model for acoustic waves propagating through a vortical flow. *J. Fluid Mech.* **823**, 658–674.

THOMAS, J., SMITH, K.S. & BÜHLER, O. 2017 Near-inertial wave dispersion by geostrophic flows. *J. Fluid Mech.* **817**, 406–438.

VAN DYKE, M. 1964 *Perturbation Methods in Fluid Mechanics*. Academic Press.

VIVANCO, F., MELO, F., COSTE, C. & LUND, F. 1999 Surface wave scattering by a vertical vortex and the symmetry of the Aharonov-Bohm wave function. *Phys. Rev. Lett.* **83**, 1966–1969.

WEI, J.-Y., LIU, J.-Y., MAHMOOD, W. & ZHAO, Q. 2017 Scattering of electromagnetic wave by vortex flow. *Phys. Lett.* A **381**, 1463–1469.